A Review and Unifying Analysis of Defect Decoration and Surface Polishing by Chemical Etching in Silicon Processing†

Milind S. Kulkarni

MEMC Electronic Materials, 501 Pearl Drive, MZ 80, Saint Peters, Missouri 63376-0008

A comprehensive review of dynamics of etching and its various applications in silicon wafer processing is accomplished, and new developments are discussed. A previously proposed pseudo two-phase phenomenological model to describe the dynamics of three-phase etching is revisited and novel augmentations are proposed. Interplay between the liquid-phase transport of reagents, the silicon surface kinetics, and the formation and the transport of gaseous bubbles is quantified. Both the model and the reported data explain effects of etching on silicon-surface polishing. Recent attempts to extend the pseudo two-phase model to describe the defect decoration by acid-based etching are discussed and new modifications are proposed. Microdefect (agglomerated defect) distribution in a monocrystalline silicon wafer is identified by growing copper precipitates on the microdefects followed by surface polishing and subsequent microdefect-decorating etching, which forms the pits on the wafer known as etch-pits by a relatively rapid chemical dissolution of the precipitates. The macrodecoration of microdefects is typically realized in the absence of significant effects of the liquid-phase mass-transport. The developed phenomenological model leads to classification of etchants as either polishing or potentially decorating and to the identification of conditions necessary for an efficient microdefect decoration. The reported analytical expressions for the microdefect-decorating and the microdefect-polishing conditions are also revisited, revised, and augmented. A series of reported experiments validates the developed model.

Introduction

Acid-based etching is widely applied in the manufacture of monocrystalline silicon substrate for device fabrication. Two important applications of etching are in the surface polishing of silicon wafers to remove mechanical damage and in the characterization of the microdefects that play a critical role in device failure. In this paper, a review of the reported developments in acid-based etching is presented. Recent developments in the quantification of quality of the surface polishing and the microdefect characterization (also known as decoration) are extensively discussed, and further revisions and modifications to the published models are proposed. Thus, this paper revisits and reviews the relevant literature in the field of acid-based etching and proposes new developments based on the unpublished research of the author of this paper.

Section I: Acid-Based Etching in Surface Polishing

Semiconductor silicon substrate wafers are prepared through various chemical and mechanical processes. First, silicon single-crystal ingots are sliced into circular disks by *slicing* followed by a flattening process called *lapping* that involves scrubbing the sliced wafers using an abrasive slurry.[1] Acid-based *etching*, which is the focus of this paper, removes the mechanical damage induced during the previous shaping processes and chemically polishes the wafer surface. Various unit operations such as *polishing* and *cleaning* follow the etching before a wafer is ready for device fabrication.

The chemical etching of silicon wafers is accomplished by dipping the wafers in an etchant, which is traditionally an acidic mixture of an oxidizing agent such as nitric acid (HNO_3), a chemical dissolving agent such as hydrofluoric acid (HF), and a diluent, or a caustic solution of potassium hydroxide (KOH). Various studies in caustic crystallographic etching have been reported.[2−4] The focus of this study, however, is on various transport and kinetic effects only in the acid-based etching. The acid-based etching is reported to proceed by the following global reactions:[1]

$$\mathrm{Si} + \text{oxidant} \rightarrow \mathrm{SiO_2} + \text{gases} + \text{byproducts} \quad (1)$$

$$\mathrm{SiO_2} + 6\mathrm{HF} \rightarrow \mathrm{H_2SiF_6} + 2\mathrm{H_2O} \quad (2)$$

The most popular oxidant used is nitric acid, and hydrofluoric acid is almost always used as the dissolving agent. The actual reaction mechanism involves many elementary reactions and is quite complicated. Hydrogen and different oxides of nitrogen can evolve. Many rate equations for the dissolution of silicon wafer under different conditions have been proposed.[5−7] The chemical etching of silicon is a multiphase reaction that involves the transport of reagents in the liquid-phase and reactions on the wafer surface. Sometimes, in the design of an etcher, the identification of the rate controlling step (mass-transport versus reaction) in a heterogeneous process like this becomes more critical than the knowledge of the actual chemistry, because, to produce uniformly etched silicon wafers, a reaction-controlled etching system requires a different design from a design of a mass-transport controlled etching system. The literature on the acid-based etching of

* To whom correspondence should be addressed. E-mail: mkulkarni@memc.com.

† Written for this special issue of *Industrial & Engineering Chemistry Research* published in honor of Professor Octave Levenspiel.

10.1021/ie020716y CCC: $25.00 © 2003 American Chemical Society
Published on Web 04/18/2003

monocrystalline silicon is vast but essentially qualitative in nature. Many of the reported observations lead to contradictory conclusions, because effects of the mass-transport are not well-incorporated.

A series of experiments to quantify the mass-transport effects in etching were performed by Schwartz and Robbins.[8] By etching wafers at different temperatures, they correlated the etching rates with the temperature using the Arrhenius expression. They also attempted to identify the controlling step by the magnitude of the activation energy—a weak dependence of the mass-transport rates on the temperature explained why the activation energy for the mass-transport-influenced (not controlled) etching rates was lower than the activation energy for the reaction-influenced (not controlled) etching rates. Although not very sophisticated, this approach could be used to qualitatively recognize the rate-influencing step. Also, there is no quantitative evidence that kinetically controlled etching was achieved in these etching studies.

Bogenschütz et al., (1967), however, claimed that the temperature dependence of the mass-transport rate was similar to that of the viscosity, which can be expressed as an exponential function of the temperature, because the mass-transport rate was a function of the viscosity. Since the mass-transport is a function of many temperature-dependent parameters other than the viscosity, this argument is not entirely valid. It, however, seems that it is an accepted approach to recognize that the rate-controlling step is based on the magnitude of the activation energy. This approach is useful for a qualitative understanding of the etching process.

A series of papers on the acid etching of silicon were published by Robbins and Schwartz, from 1958 to 1976.[8,10−12] They concluded that, for the low HF and the high HNO_3 concentrations, the etching process is greatly influenced by the diffusion of reagents in the liquid layer close to the reacting surface. Significant mass-transport effects have been reported even for the low nitric acid concentrations when the autocatalytic oxidation−reduction reaction could supposedly influence the etching rate.[10,12] These claims were supported by the observations of Bogenschütz et al. and Klein and D'Stefan, among many others.[9,13] Bogenschütz et al. showed that the activation energy for the viscosity was comparable to the "activation energy" for the mass-transport controlled etching.[11] Klein and D'Stefan observed a change in the etching rate with a change in the liquid (etchant) mixing rate.[13] In the range of HF concentrations studied, they observed a decrease in the dependence of the etching rate on the mixing rate with an increase in the HF concentration. This dependence was monotonic and linear. A process for the chemical etching of silicon wafers where nitrogen bubbling could be used for uniform mass-transport effects was described by Erk and Vandamme.[14]

Various prior as well as recent studies indicate a very strong transport effect on etching. The effect of stirring and, hence, the transport was reported to have a significant effect on the saturation current density of an n-type Si electrode.[15] Nahm et al. and Schimmel and Elkind reported a qualitative relationship between the HF and/or oxidant concentration on the formation mechanism of stains in etching.[16,17] Fathauer et al. studied visible luminescence from silicon wafers subjected to the etching processes producing stains.[18] Gaffney and Chiou reported mass-transport effects in a nitric−hydrofluoric−acetic acid system.[19] Bauer et al. recognized the importance of fluid mechanics in the acid etching.[20] No phenomenological explanation or quantification for the results observed, however, was provided. The effect of the HF concentration on the surface morphology of the etched substrate was reported by studies in the acid etching of materials other than silicon.[21] McAndrews and Sukanek postulated that, in the device etching with HF, air bubbles could be trapped and cause surface irregularities.[22] They, however, did not consider the possibility of formation of bubbles by an etching reaction or the resistance of these bubbles for the transport. As the spray etching of silicon studied by John and McDonald seems to suggest, performance of etching is a strong function of the equipment used.[23] This leads to the conclusion that the mass-transport effects are quite significant in the acid etching and many surface characteristics cannot be simply explained by studying the chemical kinetics alone, without taking transport effects into account. Osseo-Asare et al. studied the thermodynamic dissolution windows for wet chemical processing of a dilute aqueous Si−F system, but the effect of molecular transport to the reaction sites remained unanswered.[24]

Monk et al. reported a shift in the controlling step, from kinetics (reaction) to diffusion, in the etching of the thermal oxide by HF.[25,26] This study, however, discusses only the dissolution of the thermal oxide by HF in a two-phase system. The chemical reaction mechanism and kinetics for the hydrofluoric acid etching of silicon dioxide was also discussed and reviewed by Monk et al.[7,27] Kunii et al. studied the wet etching of silicon oxide films using a buffered HF solution.[28] They observed that the etching rate showed linear dependence on the HF concentration at lower HF concentrations and a nonlinear dependence on the HF concentration at higher HF concentrations, which, according to them, was explained by the change in the dominant reactive species. Nonuniformities in the oxide layer formed by boiling silicon wafers in HNO_3 were reported by Aoyama et al.[29] It was assumed that the nonuniformities could influence subsequent processing such as etching.

With a few exceptions, most studies discussed above do not attempt to quantify the interplay between the surface kinetics and the mass-transport. The magnitude of the mass-transport effects is not only a function of the *speed of transport*, given by a *transport time scale*, but also a function of the *speed of kinetics*, given by a *kinetic time scale*. The nature of the etched silicon wafer changes with any change in the kinetic mechanism as well as in the transport properties. Kulkarni and Erk presented a set of experimental data and analyzed it using a novel phenomenological model for heterogeneous reactions.[30] The data collected are consistent with the proposed phenomenological model for heterogeneous reactions and can explain various aspects of silicon surface characteristics. The proposed model explains different characteristics of an etched silicon wafer surface that earlier studies did not explain. In the first section of this paper, the work of Kulkarni and Erk (2000) and new unpublished augmentations by the author of this paper to the models proposed by them are discussed in detail.

Two-Phase System: Quantification of Process Time Scales. Chemical etching of silicon wafers is a three-phase system that involves the liquid-phase trans-

port of reactants from the bulk liquid to the wafer surface, the surface reactions that generate products in both the liquid-phase and eventually the gas-phase, and subsequent transport of products into the bulk liquid.[30] For the sake of simplicity, first, effects of eventual gaseous products on the surface morphology are neglected and a simple two-phase solid−liquid reaction system is treated (Figure 1a). The etching dynamics involving the formation of the gaseous bubbles is treated later in this study. In a two-phase system, according to the classical film-transport theory, the transport of reagents occurs by molecular diffusion through a liquid film, known as the *concentration boundary layer* or the *mass-transport film*, on the wafer surface, and thus the mass-transport rate per unit area of the wafer is defined as[30−33]

$$r_{\mathrm{m},i} = \frac{D_{\alpha,i}}{\delta_i}(C_{\mathrm{b},i} - C_{\mathrm{f},i}) \tag{3}$$

where r_{m} (mol/m^2·s) is the rate of transport of a given reagent per unit surface area, D (m^2/s) is the diffusivity of a given reagent in the liquid film, δ (m) is the liquid film thickness, and C (mol/m^3) is the concentration of a given reagent. The subscript "m" denotes the mass-transport, "b" refers to the bulk liquid conditions, "f" refers to the wafer surface conditions, and "i" identifies the reagent. The parameters subscripted by "α" indicate the influence of the molecular transport. Contributions to the mass-transport from other phenomena are discussed later in the analysis of a three-phase system. The rate of consumption of a given reagent by the surface reactions per unit area is given by

$$r_{\mathrm{r},i} = f_{\mathrm{r}}(T, C_{\mathrm{f},i}, C_{\mathrm{f},j}, C_{\mathrm{f},k}...) \tag{4}$$

where r_{r} (mol/m^2·s) is the rate of consumption (not rate of formation) of a given reagent per unit area, T (K) is the absolute temperature, and f_{r} is a function describing the surface kinetics. The subscript "r" refers to the reaction or kinetics, and the subscripts j, k... denote relevant species on the wafer surface that take part in the etching reactions.

It can be shown that, at pseudo-steady state, the overall rate of etching is given by

$$r_i = r_{\mathrm{m},i} = r_{\mathrm{r},i} = \frac{F_{\mathrm{o},i}}{R_{\mathrm{o},i}} = \frac{F_{\mathrm{m},i}}{R_{\mathrm{m},i}} = \frac{F_{\mathrm{r},i}}{R_{\mathrm{r},i}}$$

$$\text{and} \qquad R_{\mathrm{o},i} = R_{\mathrm{m},i} + R_{\mathrm{r},i} \tag{5}$$

where

$$F_{\mathrm{o},i} = C_{\mathrm{b},i},\ F_{\mathrm{m},i} = C_{\mathrm{b},i} - C_{\mathrm{f},i},\ F_{\mathrm{r},i} = C_{\mathrm{f},i},$$

$$R_{\mathrm{m},i} = R_{\alpha,i} = \frac{\delta_i}{D_{\alpha,i}}, \quad \text{and} \quad R_{\mathrm{r},i} = \frac{1}{\dfrac{f_{\mathrm{r}}(T, C_{\mathrm{f},i}, C_{\mathrm{f},j}, C_{\mathrm{f},k}...)}{C_{\mathrm{f},i}}}$$

Here, r_i (mol/m^2·s), the overall rate of the consumption of a reagent i, is given as the ratio of a driving force, F (mol/m^3), to a resistance, R (s/m). The driving force and the resistance can be based on only the mass-transport, only the kinetics, or both. Since the molecular diffusion is the only mode of the mass-transport considered, the resistance based on the mass-transport is equal to the resistance based on the molecular diffusion. The subscript "o" indicates the overall effect of the kinetics as well as the mass-transport. Figure 1b describes the phenomenological etching model discussed so far.

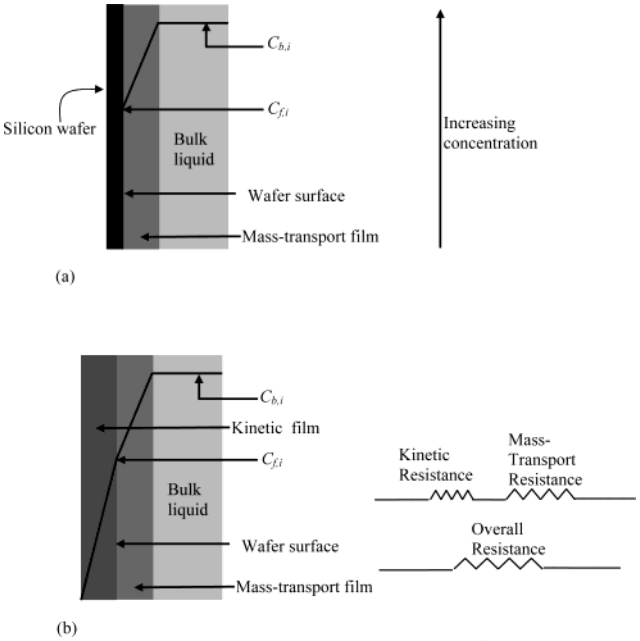

Figure 1. Phenomenological representation of the two-phase etching system depicting (a) the mass-transport resistance and (b) the kinetic and the mass-transport resistances.

The rate of decrease in the wafer thickness and the rate of the consumption of a reactant are related by stoichiometry of the etching reactions and the wafer density,

$$u = \frac{n_{\mathrm{i}}}{\rho_{\mathrm{molar}}} r_i = \xi_i r_i \tag{6}$$

where u (m/s) is the rate of decrease (not the rate of increase) in the wafer thickness or *the linear removal rate*, n_i is the number of moles of silicon (or reacting solid) reacted per mole of reactant i consumed, ρ_{molar} (mol/m^3) is the molar density of silicon (or reacting solid), and ξ (m^3/mol) is the conversion factor. With eqs 5 and 6, the resistances based on the rate of decrease in the wafer thickness are given by

$$u = \frac{F_{\mathrm{o},i}}{\beta_{\mathrm{o},i}} = \frac{F_{\mathrm{m},i}}{\beta_{\mathrm{m},i}} = \frac{F_{\mathrm{r},i}}{\beta_{\mathrm{r},i}} \quad \text{and} \quad \beta_{\mathrm{o},i} = \beta_{\mathrm{m},i} + \beta_{\mathrm{r},i} \tag{7}$$

where

$$\beta_{\mathrm{o},i} = \frac{R_{\mathrm{o},i}}{\xi_i},\ \beta_{\mathrm{m},i} = \beta_{\alpha,i} = \frac{R_{\mathrm{m},i}}{\xi_i}, \quad \text{and} \quad \beta_{\mathrm{r},i} = \frac{R_{\mathrm{r},i}}{\xi_i}$$

β (mol·s/m^4) is the resistance based on the rate of decrease in the wafer thickness.

Resistance is a quantitative measure of the time scale of a process. Thus, the *mass-transport resistance*, or simply, the *transport resistance*, reflects the mass-transport time scale, the *kinetic resistance* reflects the surface kinetic time scale, and the *overall resistance* reflects the time scale of the overall process. It is clear from eqs 5 and 7 that the overall resistance of the process is a linear combination of the kinetic resistance and the mass-transport resistance. Since etching takes place through a mass-transport step and a kinetic step, the rate-controlling step is determined by the magnitude

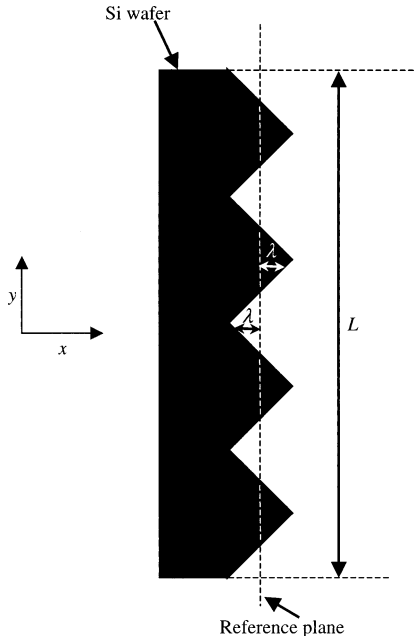

Figure 2. Schematic representation of the roughness. Note that λ is the local distance between any location on the wafer surface, not just the lowest and the highest locations, and the mean reference plane (line).

of the ratio of the mass-transport resistance to the kinetic resistance.

Application of the Resistances and the Quantification of Surface Polishing. One goal of etching is to reduce the surface roughness of wafers. The roughness is a measure of nonuniformity of the surface represented as a field of peaks and valleys (or troughs) (Figure 2) and is defined as

$$\phi = \frac{\int_0^L \lambda \, \mathrm{d}y}{\int_0^L \mathrm{d}y} \tag{8}$$

where ϕ (m) is the arithmetic length averaged roughness, L (m) is the total length under consideration, y (m) is the local position, and λ (m) is the local distance between any location on the wafer surface (not just the lowest and the highest locations) and the mean reference plane (line). Note that λ is not a periodic function of y as Figure 2 indicates for simplicity. The rate of polishing or reduction in the surface roughness can be quantified for a generic case using the classical film theory. As shown in Figure 3, let a rough silicon wafer surface be covered by a mass-transport film, through which both reactants and products are transported. It is assumed that etching takes place predominantly in the $-x$ direction. The polishing rate is defined as

$$-\frac{\mathrm{d}h}{\mathrm{d}t} = (u_\mathrm{p} - u_\mathrm{v}) \tag{9}$$

where h (m), the average distance between the peaks and the valleys, is a measure of the surface roughness. The subscripts "p" and "v" indicate the peaks and valleys (troughs), respectively. The maximum polishing rate is achieved when the linear removal rate at the valleys, u_v, is equal to zero.

$$\left[-\frac{\mathrm{d}h}{\mathrm{d}t}\right]_\mathrm{max} = u_\mathrm{p} \tag{10}$$

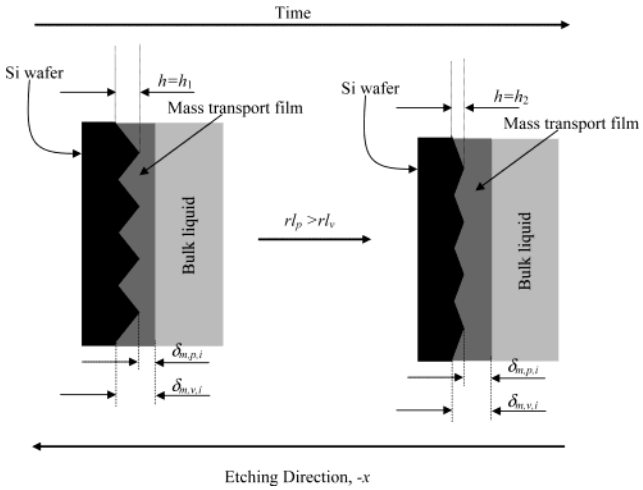

Figure 3. Schematic representation of the surface polishing in the presence of the mass-transport film.

The polishing efficiency is defined as the ratio of the actual rate of polishing to the maximum possible rate of polishing, that is, it is equal to the ratio of the difference between the etching rate at the peaks and the etching rate at the valleys to the etching rate only at the peaks:

$$\eta = \frac{-\frac{\mathrm{d}h}{\mathrm{d}t}}{\left[-\frac{\mathrm{d}h}{\mathrm{d}t}\right]_\mathrm{max}} = 1 - \frac{\beta_{\mathrm{r,p},i}}{\beta_{\mathrm{r,v},i}}\left[\frac{1+\frac{\beta_{\mathrm{m,p},i}}{\beta_{\mathrm{r,p},i}}}{1+\frac{\beta_{\mathrm{m,v},i}}{\beta_{\mathrm{r,v},i}}}\right] = 1 - \frac{\xi_{\mathrm{v},i}}{\xi_{\mathrm{p},i}}\frac{R_{\mathrm{r,p},i}}{R_{\mathrm{r,v},i}}\left[\frac{1+\frac{R_{\mathrm{m,p},i}}{R_{\mathrm{r,p},i}}}{1+\frac{R_{\mathrm{m,v},i}}{R_{\mathrm{r,v},i}}}\right] \tag{11}$$

It must be noted that the stoichiometry of the reaction remains the same for both the peaks and the valleys, and hence, $\xi_{\mathrm{v},i}/\xi_{\mathrm{p},i}$ is equal to 1. The average polishing efficiency is the integral average of the instantaneous polishing efficiency and is calculated as follows:

$$\eta_\mathrm{avg} = \frac{\int_{h_1}^{h_2}\eta \, \mathrm{d}h}{\int_{h_1}^{h_2}\mathrm{d}h} = \frac{\int_{h_1}^{h_2}\left(-\frac{\mathrm{d}h}{\mathrm{d}t}\middle/\left[-\frac{\mathrm{d}h}{\mathrm{d}t}\right]_\mathrm{max}\right)\mathrm{d}h}{\int_{h_1}^{h_2}\mathrm{d}h} = \frac{\int_{h_1}^{h_2}\frac{u_\mathrm{p}-u_\mathrm{v}}{u_\mathrm{p}}\,\mathrm{d}h}{\int_{h_1}^{h_2}\mathrm{d}h} \tag{12}$$

For a simple case of a first-order kinetics and a fixed mass-transport film thickness on valleys, the average polishing efficiency to achieve a completely flat surface is derived by solving eq 12 as

$$\eta_\mathrm{avg} = \frac{\frac{h_1}{\delta_{\mathrm{v},i}}}{2\left(1+\frac{\beta_{\mathrm{r},i}}{\beta_{\mathrm{m,v},i}}\right)} \text{ for } \delta_{\mathrm{v},i} \geq h_1, \text{ and } h_2 = 0 \tag{13}$$

where the subscripts "1" and "2" denote the initial and the final conditions, respectively. A numerical estima-

tion of the average polishing efficiency may become necessary for a more complex etching kinetics.

Equations 11 and 12 clearly demonstrate the significance of the liquid-phase diffusion on the polishing efficiency. It is evident that the surface polishing takes place only in the presence of the mass-transport effects. Most of the etching systems are designed to achieve a fixed reduction in the surface roughness for a desired removal. The ratio of the change in the surface roughness to the removal is directly measured by the polishing efficiency. Thus, understanding the dependence of the polishing efficiency on hydrodynamic conditions in the etching reactor is of primary significance.

Analysis of Surface Polishing. Equation 11 describes the generic effect of the mass-transport and the surface kinetics in any etching process. Insight into the role of the transport on surface polishing, however, is better achieved by analyzing three limiting cases, each representing a popular industrial practice for varying the polishing efficiency. The following discussion describes a typical etching system following a reasonably real kinetics, although it can be extended to any generic case. Henceforward, the terms mass-transport and transport are used interchangeably to mean the same phenomenon.

Limiting Case 1: Varying Mass-Transport Film Thickness. The mass-transport time scale and the mass-transport resistance each increase with the increasing thickness of the transport film. The thickness of this film is a function of the etchant composition and the hydrodynamic conditions in the etching reactor. The transport-film thickness decreases with increasing mixing intensity in a reactor.[32,33] Consider a hypothetical scenario at a very high liquid mixing intensity in the etching reactor, shown in Figure 4a. The mass-transport resistance is zero, the etching is kinetically controlled, and the polishing efficiency is zero.

$$\lim_{\beta_{m,p,i}\to 0,\beta_{m,v,i}\to 0} \eta = 1 - \frac{R_{r,p,i}}{R_{r,v,i}} = 1 - \frac{\beta_{r,p,i}}{\beta_{r,v,i}} = 0 \quad (14)$$

As the mixing intensity in the reactor gradually decreases, liquid cells in the shallow valleys can develop, while peaks are still open to the bulk liquid as shown in Figure 4b. These cells can be represented as a film that covers part of the surface. Under this condition, the polishing efficiency is given by

$$\eta = 1 - \frac{R_{r,p,i}}{R_{r,v,i}}\left[\frac{1}{1 + \frac{R_{m,v,i}}{R_{r,v,i}}}\right] = 1 - \frac{\beta_{r,p,i}}{\beta_{r,v,i}}\left[\frac{1}{1 + \frac{\beta_{m,v,i}}{\beta_{r,v,i}}}\right] \quad (15)$$

As the size of the liquid cells increases, the mass-transport resistance at the valleys ($R_{m,v,i}$) increases, and this change in the mass-transport resistance dominates any change in the kinetic resistance. Thus, the polishing efficiency increases as the transport effects in the shallow valleys increase. The polishing efficiency is maximum when the entire surface except the peaks is covered by the transport film (Figure 4c), a condition given by the following equations:

$$\delta_{v,i} = h \text{ and } \delta_{p,i} = 0 \quad (16)$$

The maximum polishing efficiency is given by eqs 15 and 16.

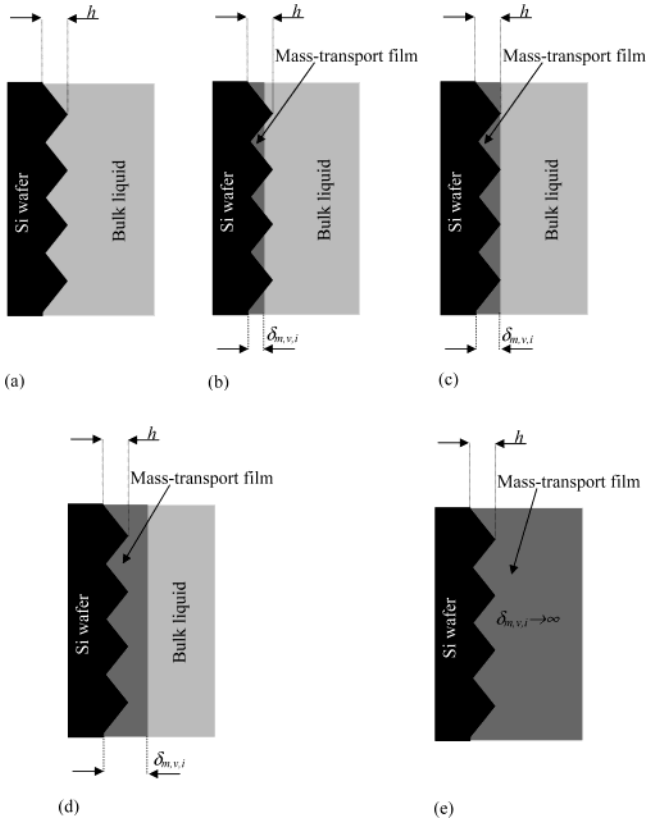

Figure 4. Schematic representation of etching (a) in the absence of the mass-transport film, (b) with liquid cells in the surface valleys, (c) at the maximum polishing efficiency, (d) in the presence of a mass-transport film of finite thickness, and (e) in the presence of an infinitely thick transport film.

When the transport film covers the entire surface as shown in Figures 4d and 3 as a result of a further decrease in the mixing intensity, the polishing efficiency is given by eq 11. It can be deduced from eq 11 that the polishing efficiency decreases as the film thickness increases and approaches an asymptotic value of zero for an infinitely thick film (Figure 4e).

$$\lim_{\delta_{p,i}\to\infty,\delta_{v,i}\to\infty} \eta = \lim_{\delta_{p,i}\to\infty,\delta_{v,i}\to\infty}\left(1 - \frac{\delta_{p,i}}{\delta_{v,i}}\right) = \lim_{\delta_{p,i}\to\infty,\delta_{v,i}\to\infty}\left(1 - \frac{\delta_{p,i}}{\delta_{p,i} + h}\right) = 0 \quad (17)$$

Figure 5 shows a typical qualitative dependence of the polishing efficiency on the ratio of the mass-transport resistance to the kinetic resistance, $\beta_{m,v,i}/\beta_{r,v,i}$. It must be noted that as this ratio changes, the kinetic resistance at peaks and that at valleys can also change. It is clearly shown here that the quality of surface polishing is a strong function of the interplay between the mass-transport and the surface kinetics. The desired etching conditions must be determined on the basis of this relationship.

Limiting Case 2: Varying Diffusivity. Addition of an inert viscous thickener to the etchant typically changes the diffusivity of the key reagent. The mass-transport time scale increases with decreasing diffusivity. Thus, the polishing efficiency is affected by the diffusivities of reactants for a fixed transport-film thickness. Consider the hypothetical scenario shown in Figure 6. Figure 6a depicts the case for the infinite diffusivity. When the diffusivity is infinite, the thickness of the

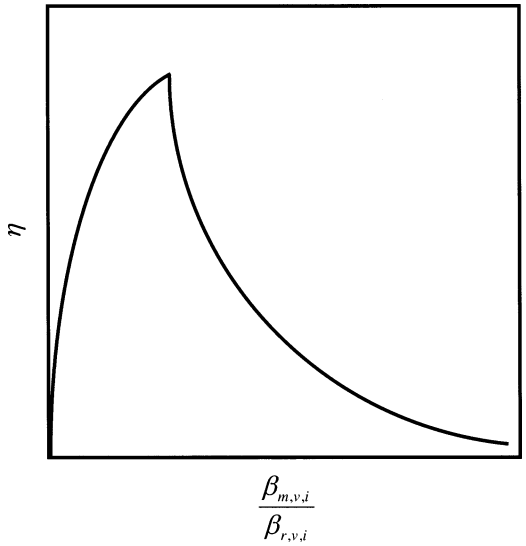

Figure 5. Typical dependence of the surface-polishing efficiency on the interplay between the mass-transport and the surface kinetics—the case of varying mass-transport film thickness.

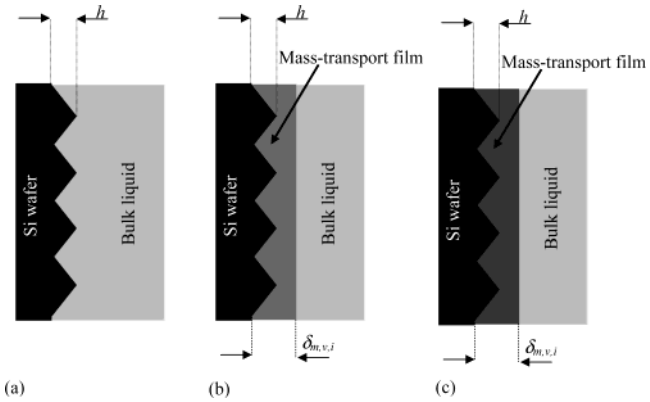

Figure 6. Schematic representation of etching (a) for the infinite diffusivity of the key reactant or for the infinite kinetic resistance, (b) for a finite diffusivity or for a finite kinetic resistance, and (c) for a negligible diffusivity or for a negligible kinetic resistance.

mass-transport film is irrelevant as the mass-transport resistance is zero. Under these conditions, the polishing efficiency is zero. When the diffusivity of the key reactant decreases (Figure 6b), the polishing efficiency increases, for a given thickness of the mass-transport film. For these conditions, the polishing efficiency is quantified by eq 11. As the diffusivity approaches zero (Figure 6c), the polishing efficiency tends to the nonzero asymptotic value described below by eq 18:

$$\lim_{D_{\alpha,i}\to 0} \eta = 1 - \frac{\delta_{\mathrm{p},i}}{\delta_{\mathrm{p},i} + h} \tag{18}$$

Thus, when the thickness of the transport film is finite, an increase in the transport resistance invariably improves the polishing quality.

The effects of the transport and the kinetics on the surface polishing can be illustrated on a graph of the polishing efficiency (η) versus the ratio of the mass-transport resistance to the kinetic resistance ($\beta_{\mathrm{m,v,}i}/\beta_{\mathrm{r,v,}i}$), for a given thickness of the mass-transport film. Figure 7 qualitatively shows the monotonic increase in the polishing efficiency with an increase in this ratio.

Limiting Case 3: Varying Kinetic Resistance. The resistance of a nonlinear kinetics can vary with the

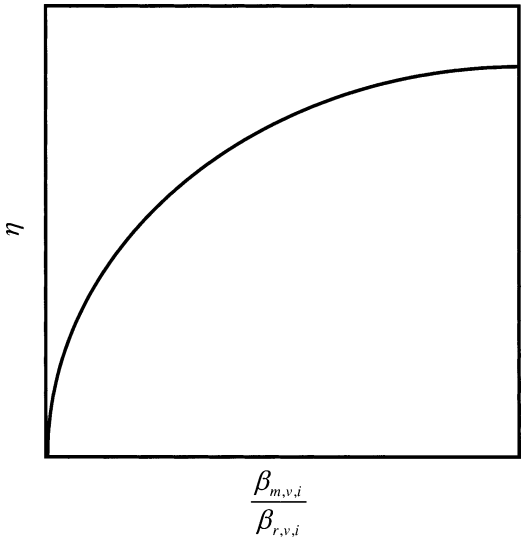

Figure 7. Typical dependence of the surface-polishing efficiency on the interplay between the mass-transport and the surface kinetics—the case of varying diffusivity of the key reactant.

concentrations of the key reactants. The effect of the kinetic resistance is similar to the effect of the diffusivity for a fixed transport film thickness. As in the case of the varying diffusivity, Figure 6 can describe the effect of a hypothetical varying kinetic resistance. The case for the infinite kinetic resistance is depicted in Figure 6a. For this case, the thickness of the mass-transport film is irrelevant as etching is kinetically controlled and the polishing efficiency is zero. As the kinetic resistance decreases (Figure 6b), the polishing efficiency increases and is given by eq 11. As the kinetic resistance approaches zero, the polishing efficiency reaches its maximum value described by eq 18 where the condition of diffusivity tending to zero is replaced by the condition of kinetic resistance tending to zero.

$$\lim_{R_{\mathrm{r,p},i}\to 0, R_{\mathrm{r,v},i}\to 0} \eta = 1 - \frac{\delta_{\mathrm{p},i}}{\delta_{\mathrm{p},i} + h} \tag{19}$$

The effects of the kinetic resistance can be captured on a graph of the polishing efficiency versus the ratio of the mass-transport resistance to the kinetic resistance, for a given thickness of the mass-transport film (Figure 8). The effect of the kinetic resistance on the polishing efficiency is similar to the effect of the diffusivity.

A Phenomenological Pseudo Two-Phase Model of Etching. Acid etching of silicon wafers is greatly influenced by the gaseous bubbles formed by the reaction products sparingly soluble in the acid mixture. In the phenomenological model presented in the previous section, the effect of the gaseous bubbles on the etching dynamics was not addressed. Macro-modeling of etching must incorporate the transport of the reagents (reactants and products) in the liquid-phase between the bulk solution and the wafer surface, the effective reaction(s) on the wafer surface, the formation and the detachment of the gaseous bubbles from the surface, and the transport of these bubbles to the bulk-phase.

NO_x and hydrogen are typically produced by the etching reactions. These gases form bubbles that adhere to the silicon surface for a finite period of time before they are dislodged. The etching reaction cannot take place on the sites masked by the bubbles. The masking

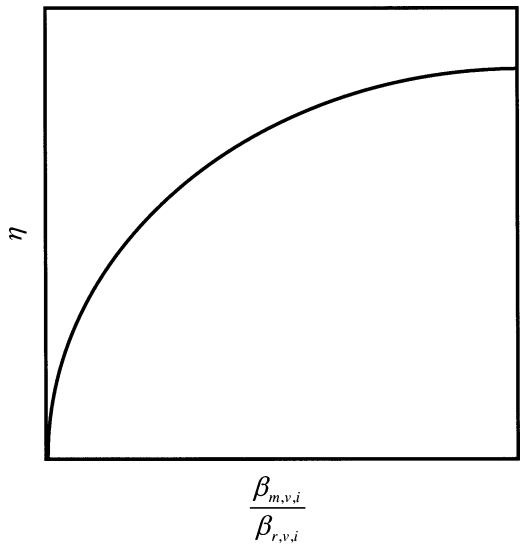

Figure 8. Typical dependence of the surface polishing efficiency on the interplay between the mass-transport and the surface kinetics—the case of varying kinetic resistance. The kinetic resistance and the diffusivity of the key reactant affect the polishing efficiency in a similar fashion (Figures 7 and 8).

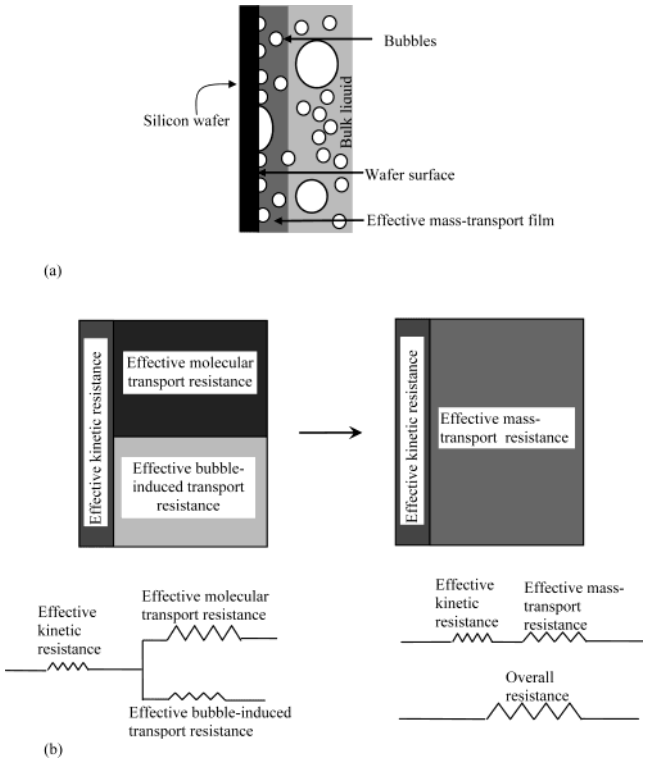

Figure 9. (a) Schematic representation of the effect of the bubbles in etching. (b) Phenomenological model that incorporates the effect of the bubbles in etching.

effect of the bubbles, henceforward called the *bubble masking*, influences the overall rate of etching and also affects the surface morphology. The bubbles dislodged from the surface disturb the liquid covering the surface, and, hence, the classical film does not exist. An effective concentration boundary layer of thickness $\delta_{\text{eff},i}$, through which a meaningful time-averaged concentration variation exists, however, can be defined. Figure 9a shows a schematic representation of the silicon surface, at any time, during an etching process. In a phenomenological sense, the system can be modeled as an effective reaction−diffusion system involving a reaction front defined by the wafer surface, a fraction of which is covered by the bubbles, and a liquid-phase mass-transport layer, properties of which are altered by the bubbles passing through it. Thus, an overall process resistance, given by an *effective kinetic resistance* and an *effective mass-transport resistance* acting in series with each other, can be defined as follows:

$$\beta_{\text{o,eff},i} = \beta_{\text{r,eff},i} + \beta_{\text{m,eff},i} \tag{20}$$

where subscript "eff" describes the effective phenomenological parameters. The transport through the effective film takes place by contributions from the molecular diffusion and the *bubble-induced diffusion* or dispersion. These two modes of transport act in parallel with each other. Thus, the effective mass-transport resistance can be defined on the basis of the parallel contributions coming from the *effective molecular transport resistance* and the *effective bubble-induced transport resistance.*

$$\beta_{\text{m,eff},i} = \frac{1}{\frac{1}{\beta_{\text{m,eff}-\alpha,i}} + \frac{1}{\beta_{\text{m,eff}-\text{g},i}}} = \frac{\beta_{\text{m,eff}-\alpha,i}\beta_{\text{m,eff}-\text{g},i}}{\beta_{\text{m,eff}-\alpha,i} + \beta_{\text{m,eff}-\text{g},i}} \tag{21}$$

where the subscript "eff−α" denotes the effective molecular transport and "eff−g" denotes the effective bubble-induced transport. The dash is used to group closely related subscripts, for the sake of simplicity. It must be noted that all transport-related effective resistances discussed above refer to the transport of species *i* through the phenomenological transport film. Figure 9b shows the relationship between various effective resistances.

The transport-related effective resistances and the effective kinetic resistance can be estimated by building various phenomenological models, many of which require rigorous analysis. The purpose of this study is not the estimation of these parameters but to gain a physical insight into dynamics of etching. Therefore, a simple analysis based on various approximations described below suffices.

Analysis of the Effective Resistances. A true steady state does not exist in a real etching system. For a fixed bulk liquid composition, at a given surface site, the actual etching rates fluctuate around a time-averaged value. Effective (linear) etching rates can be defined on the basis of the total removal of silicon:

$$u_{\text{eff}} = \frac{M(\tau)}{\rho_{\text{mol}}\tau} \tag{22}$$

where $M(\tau)$ is the mass of silicon etched per unit area (mol/m^2) over a time period τ (s), long enough to meaningfully average both the kinetic and the transport fluctuations. Both the bubbles and the liquid occupy the same site on the wafer surface at different instants over the period τ. If ϵ is the fraction of this period occupied by the bubbles, the effective kinetics is defined as

$$u_{\text{eff}} = u_{\text{r,eff}} = (1-\epsilon)\gamma u_{\text{r,open}} = (1-\epsilon)\gamma\xi_i f_{\text{r}}(\overline{T}, \overline{C_{\text{f},i}}, \overline{C_{\text{f},i}}, \overline{C_{\text{f},k}}...) \tag{23}$$

Here, the subscript "open" refers to the average conditions when the site is covered by the liquid-phase. The

variable u with the subscript "r" (u_r) is the rate of reaction in terms of the linear removal of silicon (m/s). The variables averaged over the entire period τ (excluding the durations of bubble masking) are denoted by the bars on top and indicate the average conditions when the site is covered by the liquid-phase. The function f_r describes the kinetics without bubble masking, and γ is the correction factor required to estimate $u_{r,eff}$. It must be noted that an equivalent effective kinetics can also be defined by assuming a reacting surface, a time- and space-averaged fraction of which is always covered by the bubbles. Using eq 23, the effective kinetic resistance and the *open kinetic resistance* are defined as

$$u_{r,eff} = \frac{\overline{C_{f,i}}}{\beta_{r,eff,i}} \tag{24}$$

and

$$u_{r,open} = \frac{\overline{C_{f,i}}}{\beta_{r,open,i}} \tag{25}$$

where

$$\beta_{r,eff,i} = \frac{1}{(1-\epsilon)} \frac{\overline{C_{f,i}}}{\gamma \xi_i f_r(\overline{T}, \overline{C_{f,i}}, \overline{C_{f,j}}, \overline{C_{f,k}}...)} = \frac{1}{(1-\epsilon)\gamma} \beta_{r,open,i}$$

The transport of reagents is modeled using a two-step approach. In the first step, a *modified* transport dynamics (and parameter set) is defined assuming a liquid-phase periodically disturbed by the bubbles, without considering the reaction on the surface. In the second step, an *effective* transport dynamics (and parameter set) is defined considering the effect of the effective surface kinetics.

Over the entire period τ, a fixed location in the liquid near the wafer surface is occupied by both the bubbles and the liquid-phase, at different instants. No liquid-phase transport of reagents takes place through the location when it is occupied by the bubbles. When the liquid-phase occupies the location, the transport of reagents takes place by both the molecular diffusion and the bubble-induced diffusion (dispersion). The dispersion effect of a bubble spans a volume far greater than its own. Thus, the bubbles in the surrounding vicinity affect the bubble-induced diffusion or dispersion at any location. The region near the wafer surface can be viewed as a phenomenological layer alternately occupied by the gas and the liquid, through which the transport of reagents in the liquid phase occurs both by the molecular diffusion and the dispersion. Thus, the *modified diffusivity* can be defined using a first-order approximation as follows:

$$D_{mod,i} = (1-a)(pD_{\alpha,i} + q\overline{D_{g,i}}) = D_{mod-\alpha,i} + D_{mod-g,i} \tag{26}$$

where a is the fraction of the period τ during which a location in the near-surface-liquid is occupied by the bubbles, $\overline{D_{g,i}}$ is the *bubble-induced diffusivity* or the *dispersion coefficient* averaged over the cumulative duration of liquid occupancy over the period τ, and p and q are the correction factors defined to incorporate the dynamic and the geometric approximations. The subscript "mod" refers to the modified liquid-phase properties. The modified diffusivity (eq 26) can also be defined assuming that the effective film is a dynamic porous layer of a time- and space-averaged porosity, dynamics of which introduces liquid dispersion. This treatment, however, is equivalent to the one discussed here. For a surface periodically blocked by the bubbles, the effective mass-transport rate (in equivalent linear removal of silicon) is defined as

$$\begin{aligned} u_{eff} = u_{m,eff} &= \psi(1-\epsilon) u_{m,mod} \\ &= \psi(1-\epsilon)\xi_i \left[\frac{D_{mod-\alpha,i} + D_{mod-g,i}}{\delta_{eff,i}}\right](C_{b,i} - \overline{C_{f,i}}) \\ &= \psi(1-\epsilon)\xi_i \left[\frac{D_{mod,i}}{\delta_{eff,i}}\right](C_{b,i} - \overline{C_{f,i}}) \\ &= \xi_i \left[\frac{D_{eff,i}}{\delta_{eff,i}}\right](C_{b,i} - \overline{C_{f,i}}) \end{aligned} \tag{27}$$

where $u_{m,mod}$ (m/s) denotes the mass-transport rate (in equivalent linear removal of silicon) across the concentration driving force equal to $(C_{b,i} - \overline{C_{f,i}})$, in a system allowing the continuous uninterrupted transport. In the diffusion-reaction system discussed here, the consumption of reactants takes place only during $(1-\epsilon)$ fraction of the period τ, when a surface site is covered by the liquid. The effective mass-transport rate is then given by the product of the modified rate ($u_{m,mod}$), $(1-\epsilon)$, and a phenomenological correction factor, ψ, that accounts for phenomenological approximations. The effective mass-transport resistance is defined using the equation set (27) as below:

$$u_{m,eff} = \left(\frac{1}{\beta_{m,eff-\alpha,i}} + \frac{1}{\beta_{m,eff-g,i}}\right)(C_{b,i} - \overline{C_{f,i}}) = \frac{(C_{b,i} - \overline{C_{f,i}})}{\beta_{m,eff,i}} \tag{28}$$

Equation 28 satisfies the conditions set by eq 21. Additional transport-related resistances can now be defined as follows:

$$\beta_{m,eff,i} = \frac{\beta_{m,mod,i}}{\psi(1-\epsilon)} = \frac{\delta_{eff,i}}{\xi_i D_{eff,i}} = \frac{\delta_{eff,i}}{\psi(1-\epsilon)\xi_i D_{mod,i}}$$

$$\beta_{m,mod,i} = \frac{\beta_{m,mod-\alpha,i}\beta_{m,mod-g,i}}{\beta_{m,mod-\alpha,i} + \beta_{m,mod-g,i}}$$

$$\beta_{m,eff-\alpha,i} = \frac{\beta_{m,mod-\alpha,i}}{\psi(1-\epsilon)} = \frac{\delta_{eff,i}}{\psi(1-\epsilon)(1-a)\xi_i p D_{\alpha,i}}$$

$$\beta_{m,eff-g,i} = \frac{\beta_{m,mod-g,i}}{\psi(1-\epsilon)} = \frac{\delta_{eff,i}}{\psi(1-\epsilon)(1-a)\xi_i q \overline{D_{g,i}}} \tag{29}$$

Equation 29 defines a few effective resistances and a few additional *modified resistances* denoted by the subscript "mod". These additional resistances defined independent of the surface coverage by the masking bubbles, while accounting for the effect of the detached bubbles in the near-surface liquid, are the *modified molecular transport resistance* ($\beta_{m,mod-\alpha,i}$) and the *modified bubble-induced transport resistance* ($\beta_{m,mod-g,i}$). The cumulative *modified mass-transport resistance* ($\beta_{m,mod,i}$) is given by the contributions from the modified molecular transport resistance and the modified bubble-induced transport resistance. Equation 29 also defines

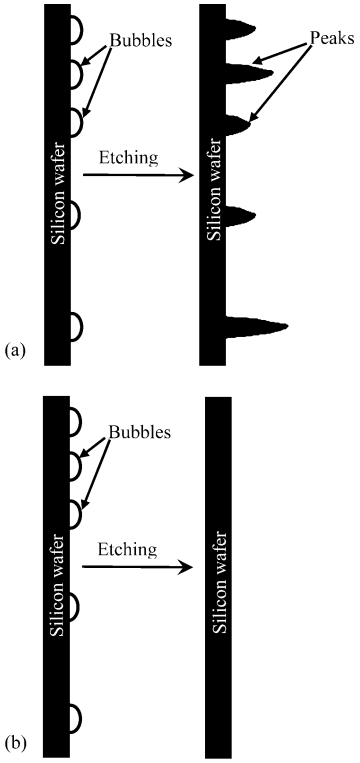

Figure 10. Etching under (a) intense bubble masking conditions (high $\beta_{rem}/\beta_{r,open,i}$) and (b) negligible bubble masking conditions (low $\beta_{rem}/\beta_{r,open,i}$).

the *effective diffusivity* as a function of the modified diffusivity and the bubble masking effect.

The developed pseudo two-phase model can be applied to describe the general behavior of a true three-phase system in many cases. Under most conditions, average etching rates can be estimated accurately by the pseudo two-phase model. Under various conditions, on a macroscale, the equation describing the polishing efficiency in a two-phase system can be applied to describe the polishing efficiency in a pseudo two-phase system by replacing the resistances of the two-phase model with the effective resistances. The applications and limitations of the pseudo two-phase model in describing a three-phase system are described in the following sections.

Effect of Bubbles on a Silicon Surface. As discussed earlier, the gaseous bubbles are formed on the surface of the reacting wafer. If the bubbles adhere to a site for an appreciable period of time, the site masked by the bubbles can form a peak as the surrounding surface is continuously etched. A representative dimensionless height (H) of the peak is given by integrating a representative removal around the masked site during a representative bubble masking period as follows:

$$H = \frac{u_{r,open} t_{mask}}{l^*} = \frac{t_{mask} \overline{C_{f,i}}}{l^* \beta_{r,open,i}} = \frac{\beta_{rem}}{\beta_{r,open,i}} \qquad (30)$$

where t_{mask} (s) is the representative bubble residence time on the surface or the *bubble masking time*, l^* is a representative length scale (m), and β_{rem} is the *bubble detachment resistance*. Equation 30 gives only a representative height of the peaks formed by the *bubble masking*. Thus, a use of representative β_{rem} and $\beta_{r,open,i}$ suffices. A peak of an appreciable height is formed if the ratio of the bubble detachment resistance to the open kinetic resistance around the site is very high. At a global level, the surface morphology of an etched wafer is affected by these local peaks and valleys as excessive bubble masking can cause increased surface disturbance. The operating region for the acceptable bubble masking intensity can be defined on the basis of industrial surface quality requirements as

$$H \le H_{bm}, \quad \text{i.e.,} \quad \frac{\beta_{rem}}{\beta_{r,open,i}} \le \left[\frac{\beta_{rem}}{\beta_{r,open,i}}\right]_{bm} \qquad (31)$$

where subscript "bm" indicates the tolerable bubble masking intensity or the bubble masking limit. A schematic description of the bubble masking is given by Figure 10a,b.

Analysis of the Pseudo Two-Phase Model. Behavior of the pseudo two-phase system is described by the equations similar to those that describe the two-phase model. Equation 11 is valid upon replacing the (two-phase) resistances with the effective resistances. Thus, the key equation describing the polishing efficiency can be rewritten as

$$\eta = \frac{-\frac{dh}{dt}}{\left[-\frac{dh}{dt}\right]_{max}} = 1 - \frac{\beta_{r,eff,p,i}}{\beta_{r,eff,v,i}} \left[\frac{1 + \frac{\beta_{m,eff,p,i}}{\beta_{r,eff,p,i}}}{1 + \frac{\beta_{m,eff,v,i}}{\beta_{r,eff,v,i}}}\right] = 1 - \frac{\xi_{v,i}}{\xi_{p,i}} \frac{R_{r,eff,p,i}}{R_{r,eff,v,i}} \left[\frac{1 + \frac{R_{m,eff,p,i}}{R_{r,eff,p,i}}}{1 + \frac{R_{m,eff,v,i}}{R_{r,eff.v,i}}}\right] \qquad (32)$$

Equation 32 describes the polishing efficiency of a generic etching system under most conditions. The prediction of the polishing efficiency is physically meaningful when the length scale of the roughness described by the distance between the two adjacent peaks in consideration is different from the length scale of the surface disturbance caused by the bubble masking. Under such a condition, the qualitative variation of the polishing efficiency as a function of the ratio of the effective mass-transport resistance to the effective kinetic resistance in a pseudo two-phase system remains similar to the qualitative variation of the polishing efficiency as a function of the mass-transport resistance to the kinetic resistance in a two-phase system, even in the presence of intense bubble masking. In the following discussion, such an assumption is made if not specified otherwise. Three limiting cases can be studied to understand the generic application of the pseudo two-phase model.

Limiting Case 1: Varying Effective Transport-Film Thickness. Varying the mixing intensity in the etching reactor varies the thickness of the effective mass-transport film. As the mixing intensity decreases, the effective film thickness increases, resulting in a higher modified mass-transport resistance, and the shear force acting on the masking bubbles decreases, resulting in a higher bubble masking time. Experimental results reported by Kulkarni and Erk indicate that etching

rates, typically, are greatly influenced by the bubble masking and that the effect of variation in the liquid mixing intensity is stronger on the bubble masking time than on the interfacial concentration of species i ($\overline{C_{f,i}}$) or on the open kinetic resistance ($\beta_{r,open,i}$).[30] Hence, from eq 30, it can be deduced that the bubble detachment resistance increases with the bubble masking time and the modified mass-transport resistance. Thus, for a fixed system (especially for a fixed surface), the condition for acceptable operation below the intense bubble masking, described by (31), can be expressed by the following inequality:

$$H \le H_{bm}, \quad \text{i.e.,} \quad \frac{\beta_{m,mod,i}}{\beta_{r,open,i}} \le \left[\frac{\beta_{m,mod,i}}{\beta_{r,open,i}}\right]_{bm,\delta} \tag{33}$$

where the subscript "δ" indicates the case of varying effective film thickness. Since eq 33 is based on qualitative arguments, only representative $\beta_{m,mod,i}$ and $\beta_{r,open,i}$ are used. The assumptions made in derivation of eq 33 are reasonably valid only in an order of magnitude analysis. Therefore, eq 33 must be treated only as an approximate guide for the industrial practice. Using eqs 25 and 29, and assuming that the product $(\psi/\gamma) \times (\beta_{m,eff,i}/\beta_{r,eff,i})$ increases with increasing $\beta_{m,eff,i}/\beta_{r,eff,i}$, the operating region can be described by the following equation:

$$H \le H_{bm}, \quad \text{i.e.,} \quad \frac{\beta_{m,eff,i}}{\beta_{r,eff,i}} \le \left[\frac{\beta_{m,eff,i}}{\beta_{r,eff,i}}\right]_{bm,\delta} \tag{34}$$

Therefore, for a given system of given surface and fluid properties, a limiting value for the ratio of the effective mass-transport resistance to the effective kinetic resistance can be defined, beyond which surface deterioration by the bubble masking dominates.

Excluding the bubble masking effect, analysis of this limiting case of the pseudo two-phase system is similar to that of the two-phase system. Equations 14−16 are valid if the effective parameters are used instead of the parameters defined in the two-phase system. Since the effective diffusivity can marginally vary between peaks and valleys, the asymptotic value of the polishing efficiency at the infinite effective film thickness is given by

$$\lim_{\delta_{p,eff,i}\to\infty,\delta_{v,eff,i}\to\infty} \eta = 1 - \frac{D_{eff,v,i}}{D_{eff,p,i}} \tag{35}$$

The ratio $D_{eff,v,i}/D_{eff,p,i}$, however, is very close to unity, and the limiting value of the polishing efficiency is approximately equal to zero. Figure 11 shows a typical dependence of the polishing efficiency on the ratio of the effective mass-transport resistance to the effective kinetic resistance, $\beta_{m,eff,v,i}/\beta_{r,eff,v,i}$. The behavior is quite similar to that of the two-phase system except for the bubble masking effect, which disturbs the surface at the bubble masking scale, beyond the limit defined by eq 34.

Limiting Case 2: Varying Effective Diffusivity. In this discussion, the thickness of the effective mass-transport film is assumed to be constant. Typically, a change in the diffusivity of a reagent in the etching mixture is a result of addition of a viscous, inert, and thick liquid known as a thickener. Before analyzing this limiting case, it is important to understand the effect of the bubble masking.

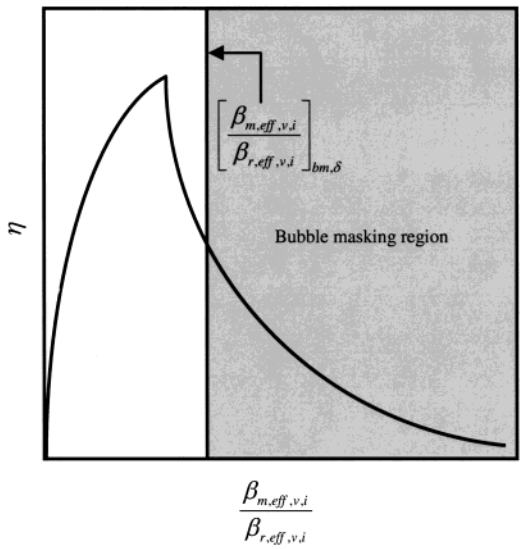

Figure 11. Typical dependence of the surface polishing efficiency on the interplay between the effective mass-transport and the effective surface kinetics for the case of varying effective mass-transport film thickness. The shaded area indicates the bubble masking region, in which the shown relationship is physically meaningful if the masking length-scale is different from the length-scale of the surface disturbance being polished.

Average bubble residence time on the wafer surface is a function of properties of the surface, gases forming the bubbles on the surface, and the liquid-phase itself. For a given system, however, all other parameters showing negligible variation, the bubble residence time on the surface increases with the increasing difficulty for a bubble to move in the liquid near the surface. The difficulty for the bubble movement increases with increasing liquid viscosity, which decreases both the molecular diffusivity and the bubble-induced dispersion. Hence, for a given system, both the modified mass-transport resistance and the bubble masking time increase with the liquid viscosity. As will be shown later in this paper, the relative effect of a change in the viscosity is greater on the bubble masking time than on the interfacial concentration of species i. Hence, the bubble detachment (removal) resistance (eq 30) increases with the increasing modified mass-transport resistance. Thus, the operating region below the bubble masking limit can be defined on the basis of the modified mass-transport resistance as follows:

$$H \le H_{bm}, \quad \text{i.e.,} \quad \frac{\beta_{m,mod,i}}{\beta_{r,open,i}} \le \left[\frac{\beta_{m,mod,i}}{\beta_{r,open,i}}\right]_{bm,D} \tag{36}$$

where the subscript "D" indicates the case of varying effective diffusivity. Again, eq 36 serves only as an approximate guide for the industrial practice as it is based on qualitative arguments and on representative $\beta_{m,mod,i}$ and $\beta_{r,open,i}$. Using eqs 25 and 29 and assuming that the product $(\psi/\gamma) \times (\beta_{m,eff,i}/\beta_{r,eff,i})$ increases with increasing $\beta_{m,eff,i}/\beta_{r,eff,i}$, this operating region is expressed as

$$H \le H_{bm}, \quad \text{i.e.,} \quad \frac{\beta_{m,eff,i}}{\beta_{r,eff,i}} \le \left[\frac{\beta_{m,eff,i}}{\beta_{r,eff,i}}\right]_{bm,D} \tag{37}$$

Equation 37 defines the bubble masking limit for any industrial etching process. It must be noted that the bubble masking limits are defined the same way for the

case of varying effective mass-transport film thickness and the case of varying effective diffusivity. Magnitudes of these limiting values, however, are different.

The behavior of the pseudo two-phase model is similar to that of the two-phase model described earlier. Equation 11 is valid upon replacing the resistances of the two-phase model with the effective resistances. Equation 18, upon replacing the parameters of the two-phase model with the effective parameters, describes the asymptotic value of the polishing efficiency when the effective diffusivity tends to zero. The effects of the transport and the kinetics on the surface polishing can be illustrated on a graph of the polishing efficiency (η) versus the ratio of effective mass-transport resistance to the effective kinetic resistance ($\beta_{m,eff,v,i}/\beta_{r,eff,v,i}$). Figure 12 shows the dependence of the polishing efficiency on this ratio. Beyond the bubble-masking limit, surface morphology is altered by the bubble masking.

Limiting Case 3: Varying Effective Kinetic Resistance. The effective kinetic resistance typically changes with the etchant composition. On the basis of the discussions for the two-phase model, it can be deduced that the effect of variation in the effective kinetic resistance on the polishing efficiency is similar to the effect of variation in the effective diffusivity, for a fixed effective mass-transport film thickness. Typically, most of the real etching systems exhibit kinetics of order greater than 1 with respect to the key reactant, HF. For such systems, the open kinetic resistance decreases with increasing HF concentration. Thus, both the ratio of the bubble detachment resistance ($\beta_{rem} = (t_{mask}\overline{C_{f,i}})/^*$) to the open kinetic resistance, $\beta_{rem}/\beta_{r,open,i}$, and the ratio of the modified transport resistance to the open kinetic resistance, $\beta_{m,mod,i}/\beta_{r,open,i}$, increase with the increasing HF concentration. Hence, for the sake of consistency with the previous cases, the operating region below the bubble masking limit for this case can also be defined by

$$H \le H_{bm}, \quad \text{i.e.,} \quad \frac{\beta_{m,mod,i}}{\beta_{r,open,i}} \le \left[\frac{\beta_{m,mod,i}}{\beta_{r,open,i}}\right]_{bm,r} \tag{38}$$

or

$$H \le H_{bm}, \quad \text{i.e.,} \quad \frac{\beta_{m,eff,i}}{\beta_{r,eff,i}} \le \left[\frac{\beta_{m,eff,i}}{\beta_{r,eff,i}}\right]_{bm,r} \tag{39}$$

Considering the approximations on which eqs 38 and 39 are based, only representative effective resistances are used.

The polishing efficiency increases monotonically with the decreasing effective kinetic resistance and reaches an asymptotic non-zero value. This behavior is captured by eq 11, upon replacing the resistances of the two-phase model with the effective resistances. Variation of the effective diffusivity from peaks to valleys, as described in the *Limiting Case 1*, can be incorporated in describing the asymptotic value of the polishing efficiency:

$$\lim_{R_{r,eff,p,i}\to 0, R_{r,eff,v,i}\to 0} \eta = 1 - \frac{D_{eff,v,i}}{D_{eff,p,i}} \frac{\delta_{eff,p,i}}{\delta_{eff,p,i} + h} \tag{40}$$

Typically, $D_{eff,v,i}/D_{eff,p,i}$ is very close to unity and, hence, can be dropped. A graph of the polishing efficiency versus $\beta_{m,eff,v,i}/\beta_{r,eff,v,i}$ captures the effect of the effective kinetic resistance (Figure 13), which is similar to the

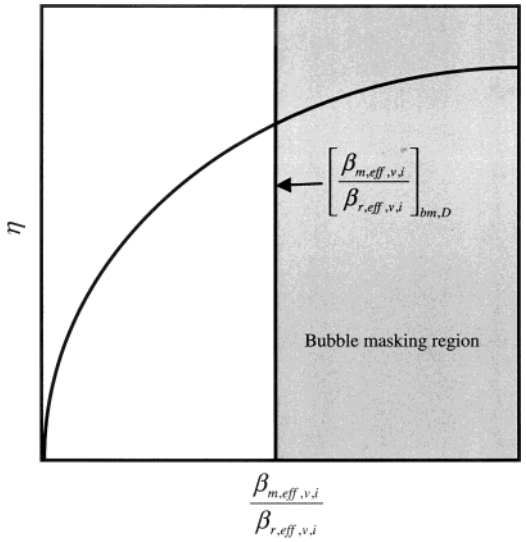

Figure 12. Typical dependence of the surface polishing efficiency on the interplay between the effective mass-transport and the effective surface kinetics for the case of varying effective diffusivity of the key reagent. The shaded area indicates the bubble masking region, in which the shown relationship is physically meaningful if the masking length-scale is different from the length-scale of the surface disturbance being polished.

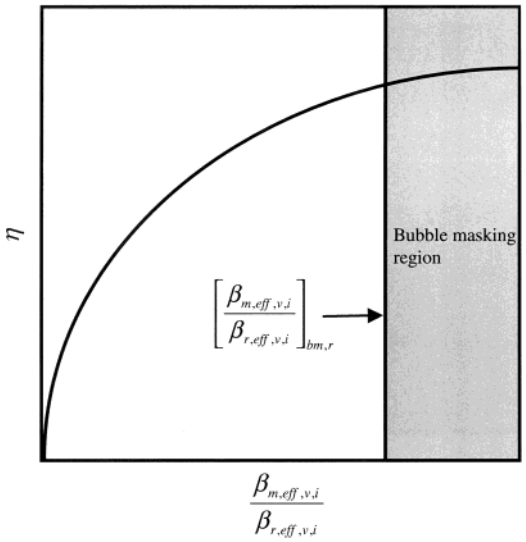

Figure 13. Typical dependence of the surface polishing efficiency on the interplay between the effective mass-transport and the effective surface kinetics for the case of varying effective kinetic resistance. The shaded area indicates the bubble masking region, in which the shown relationship is physically meaningful if the masking length-scale is different from the length-scale of the surface disturbance being polished.

effect of the effective diffusivity. In this case, however, the bubble masking limit is defined by eq 39 instead of eq 37. It must be noted that the bubble-masking limit set by eq 39 can be different from the bubble masking limit set by eq 37.

Experimental Setup. The performed experiments focus on collecting data to validate many aspects of the proposed phenomenological model, from the bubble masking to the surface polishing. Experiments were conducted in two different setups. Most of the experiments were performed using the setup shown in Figure 14a.[14] The mixture of an oxidizing acid, a dissolving acid, and diluents, collectively known as the etchant, is fed into the etcher, along with optional nitrogen gas at a high pressure. Nitrogen, when optionally introduced,

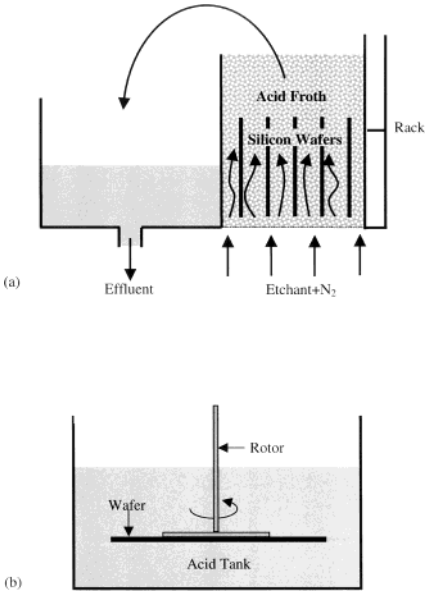

Figure 14. (a) Industrial setup used for etching multiple wafers. (b) Laboratory setup used to etch single wafers.[30] (Reproduced by permission of The Electrochemical Society, Inc.)

remains in the form of distributed bubbles. A process box containing silicon wafers is placed in the etcher as shown in the figure. The process box hosts an assembly of rotors that rotate the wafers about their centers. Silicon wafers were etched at different etchant compositions and temperatures and the data collected were analyzed using the pseudo two-phase phenomenological model.

Another setup shown in Figure 14b was also used for a few experiments involving etching single wafers. In this setup, a single wafer can be etched at different rotational speeds in an acid bath. The arrangement involves mounting the wafer on a rotating disk by applying an adhesive on the back surface of the wafer. In this setup, the adhesive glue used to mount the wafer is typically attacked by the acid, and some flakes of the glue residue are added to the acid, causing some masking effects. Hence, the surface of the etched wafer is influenced together by the glue holding the wafer and the rotating disk.

Experiments: Effect of Bubbles. In this discussion, the bubble masking at various length scales is demonstrated by a series of experiments. Various conditions leading to and reduction of the bubble masking are discussed. Surface morphologies developed by the bubble masking under various length scales are analyzed.

The Intrinsic Bubbles. The gas bubbles produced by the etching reaction (hydrogen + NO_x) are referred to as the *intrinsic bubbles*. The bubbles generated by sparging or the introduction of an inert gas into the etch bath (etching reactor) for the liquid-mixing purpose, are referred to as the *extrinsic bubbles*. The effect of the intrinsic bubbles on the surface morphology is better understood by studying the etched surface profile. Surface irregularities are also observed by using optical inspection techniques that identify peaks and valleys on the surface by shining laser beams on it and then measuring the intensity of the reflected light. One such technique involves generation of the *light-scatter picture (LSP)*, in which the peaks and the valleys on the surface are captured as spots of varying intensity (Figure 15).

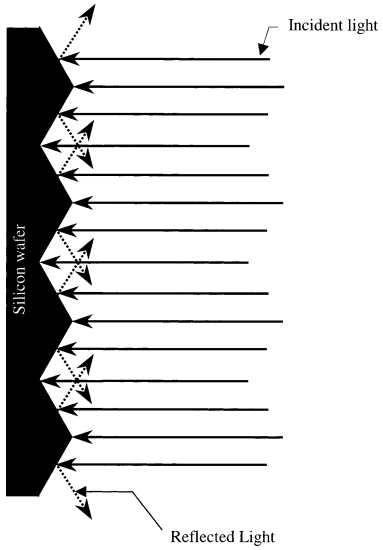

Figure 15. Schematic representation of light scattering that generates an LSP (light scattering picture).[30] (Reproduced by permission of The Electrochemical Society, Inc.)

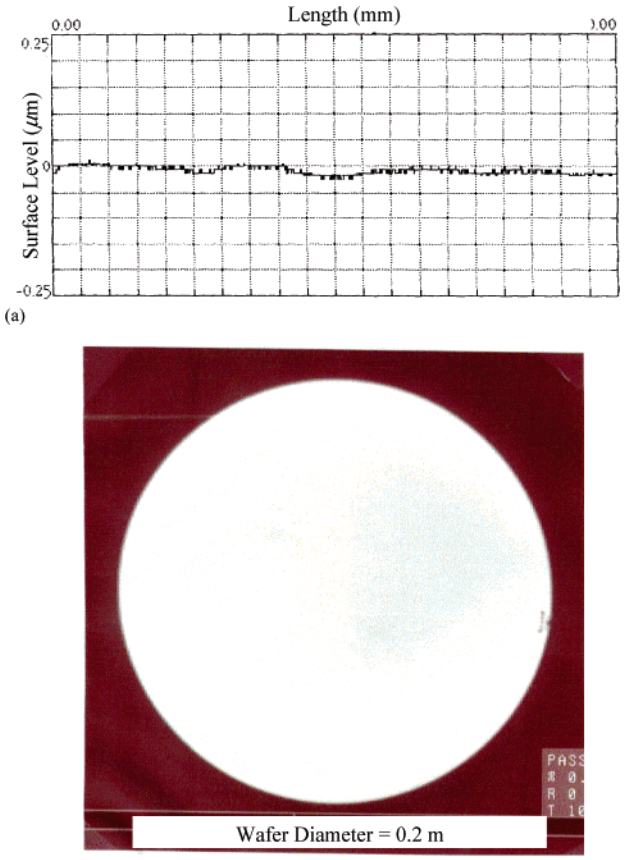

Figure 16. (a) Surface profile of a smooth polished wafer. (b) LSP of a smooth polished wafer.[30] (Reproduced by permission of The Electrochemical Society, Inc.)

The surface profile of a smooth polished silicon wafer is shown in Figure 16a. As can be observed in this figure, there are no surface irregularities detected within the resolution of the equipment. The LSP (Figure 16b) of a smooth polished wafer also shows no surface irregularities. These smooth polished wafers were then etched at 5 rpm, in a mixture of HF, HNO_3, H_3PO_4, and H_2O, in the experimental setup described in Figure 14a, without extrinsic bubbling. The surface profile and the

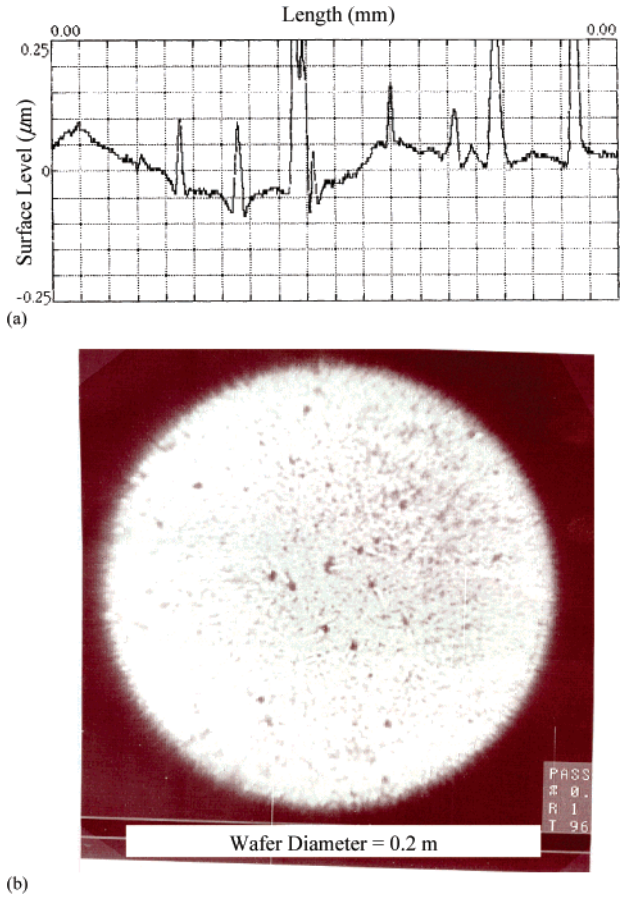

Figure 17. (a) Surface profile of an initially smooth polished wafer after etching in a mixture of HF, HNO_3, H_3PO_4, and H_2O, at 5 rpm, without extrinsic bubbling. (b) LSP of the wafer described in Figure 17a.[30] (Reproduced by permission of The Electrochemical Society, Inc.)

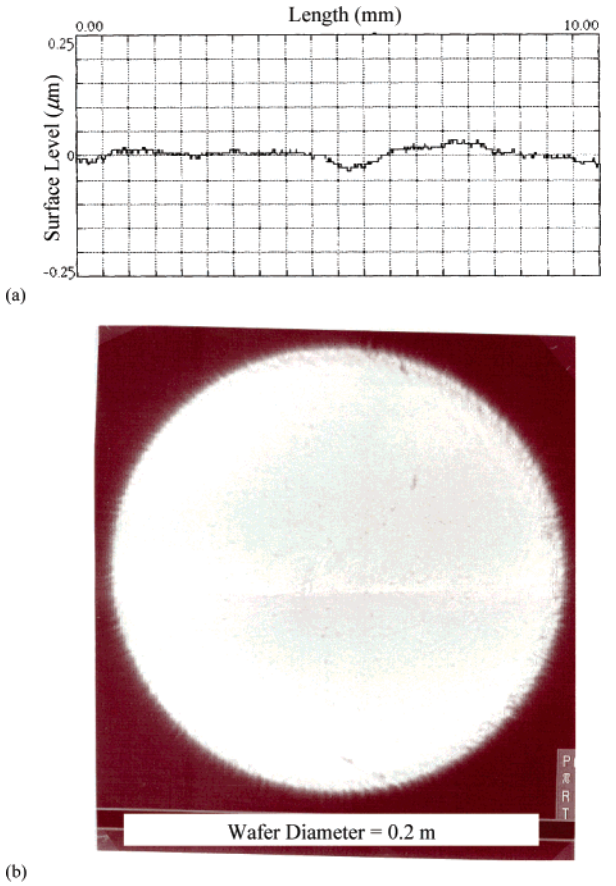

Figure 18. (a) Surface profile of an initially smooth polished wafer after etching in a mixture of HF, HNO_3, H_3PO_4, and H_2O, at 60 rpm, without extrinsic bubbling. (b) LSP of the wafer described in Figure 18a.[30] (Reproduced by permission of The Electrochemical Society, Inc.)

LSP of the etched wafer are shown in Figures 17a and 17b, respectively. The irregularities on the surfaces of the etched wafers are caused by the bubbles formed by the reaction. Since the wafer rotation speed was very low, the surface shear was very low and the effective mass-transport resistance was very high. Under these conditions, the bubble detachment resistance on the surface is very high. Hence, the bubble masking effect produced peaks during etching and resulted in a disturbed surface. Moreover, to support this argument, it is necessary to show that when the bubble detachment resistance is lower, the surface irregularities are negligible. This can be achieved by etching wafers under a higher shear force. The surface shear and the mixing intensity are increased by increasing the wafer rotational speed. Hence, the silicon wafers were etched at 60 rpm in the same acid mixture, and, the results of this experiment are shown in Figure 18a,b. The surface contour (Figure 18a) shows a negligible irregularity, and the LSP (Figure 18b) of the etched wafer shows a very smooth surface. At higher rotational speeds, the effective mass-transport resistance and the bubble detachment resistance are lower, and the etched wafers show smoother surface and minimal bubble masking effect.

To clearly demonstrate the influence of the effective mass-transport resistance on the bubble masking effect and the effect of the bubble masking on surface irregularities, a simple experiment was performed using the lab-scale setup described in Figure 14b. A polished silicon wafer was etched in a very dilute etching mixture (with negligible molar HF concentration), in the horizontal position. The wafer was etched for more than 15 μm removal, at 60 rpm. The LSP (Figure 19a) and the surface profiles at the center (Figure 19b) and at the periphery (Figure 19c) clearly show the influence of the effective mass-transport resistance on the bubble masking. In this system, during etching, the shear force and the centrifugal force at the center of the wafer are lower than those at the periphery (Levich's solution is not applicable here). Thus, both the bubble detachment resistance and the effective mass-transport resistance decrease with increasing radial distance from the center. Hence, the bubble masking effect is predominantly observed in the central region of the etched wafer, and the surface closer to the periphery is smoother (Figure 19b,c).

According to the developed pseudo two-phase model, bubble masking can be decreased by both increasing the mixing intensity in the etching liquid and decreasing the viscosity of the liquid. Results in this section show that the intensity of bubble masking does decrease with the increasing liquid mixing.

The Extrinsic Bubbles. In the industrial etcher (Figure 14a), extrinsic nitrogen bubbling can be used to achieve a more homogeneous turbulence that improves the performance of the etcher. This extrinsic bubbling also leaves its signature on the etched surface. The smooth polished wafers show a wavy pattern after etching under the extrinsic bubbling (Figure 20a,b). The extrinsic bubbles, however, impart waviness of a higher length scale and a lower frequency. The extrinsic bubbles

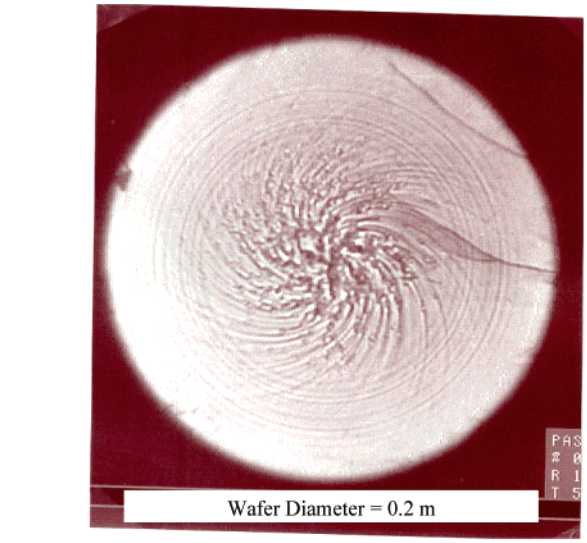

(a)

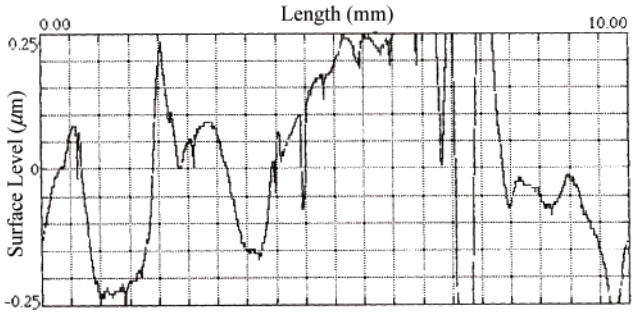

(b)

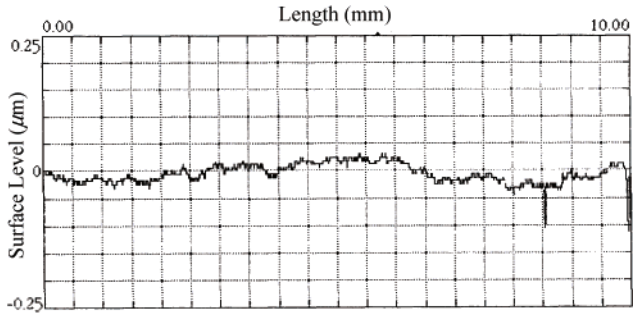

(c)

Figure 19. (a) LSP of an initially smooth polished wafer after etching in a mixture of HF, HNO_3, H_3PO_4, and H_2O, at a lower HF concentration, at 60 rpm. (b) Surface profile at the center of the wafer described in Figure 19a. (c) Surface profile at the periphery of the wafer described in Figure 19a. (Reproduced by permission of The Electrochemical Society, Inc.)

increase the mixing intensity and decrease most of the intrinsic bubble masking at length scales relevant for the roughness measurement. Hence, the extrinsic bubbles help to reduce the surface roughness, caused by the intrinsic bubble masking, at scales smaller than their own size. The surface pattern imparted by the extrinsic bubbles is a net result of a complex dynamics of intense local mixing cells created by the bubble movement and also of the short-term obstruction of the transport of reagents by the extrinsic bubble masking. This creates a more discrete pattern on the surface, analogous to the pattern on a steel sheet subject to multiple hammer strokes.

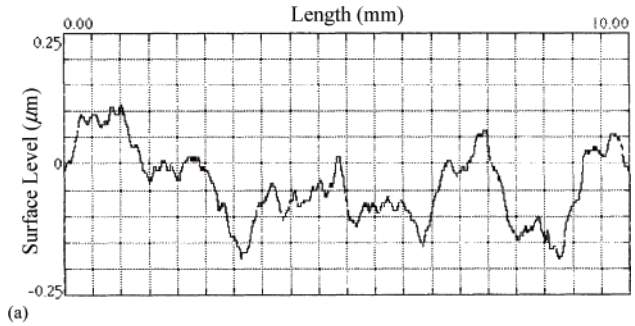

(a)

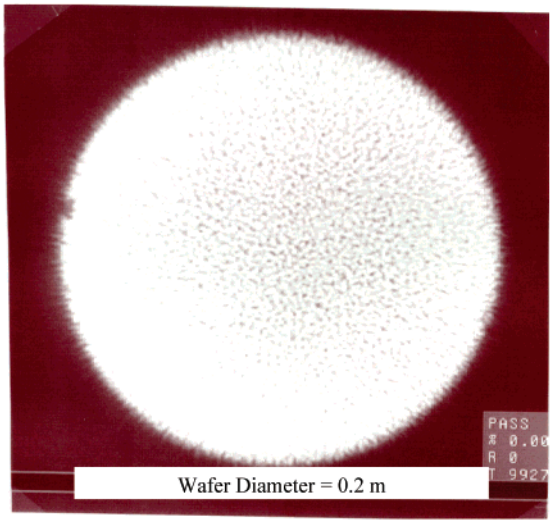

(b)

Figure 20. (a) Surface profile of an initially smooth polished wafer after etching in a mixture of HF, HNO_3, H_3PO_4, and H_2O, with extrinsic nitrogen bubbling. (b) LSP of the wafer described in Figure 21a.[30] (Reproduced by permission of The Electrochemical Society, Inc.).

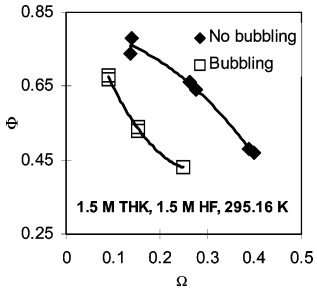

Figure 21. Effect of extrinsic bubbling on the surface roughness (etchant: HF + excess HNO_3 + H_3PO_4 + H_2O).[30] (Reproduced by permission of The Electrochemical Society, Inc.).

To study the effect of the extrinsic bubbling, rough silicon wafers with very low gloss (0−5 gloss units) and high roughness ($0.2-0.3 \times 10^{-6}$ m) were etched with and without extrinsic nitrogen bubbling in a 1.5 M HF + 1.5 M H_3PO_4 + excess HNO_3 (and water) mixture. Figure 21 shows the dimensionless roughness (Φ) of the etched wafers as a function of the dimensionless removal (Ω) by etching. Improvement (reduction) in the roughness is very poor in the absence of the extrinsic bubbling, when the intrinsic bubble masking effect is present. The intrinsic bubble masking is lower when the extrinsic bubbling is present, and hence, the polishing efficiency and the reduction in roughness are higher in the presence of the extrinsic bubbling.

The extrinsic bubbles impinging on the wafer surface reduce the intrinsic bubble masking and produce a surface disturbance of a length scale different from the

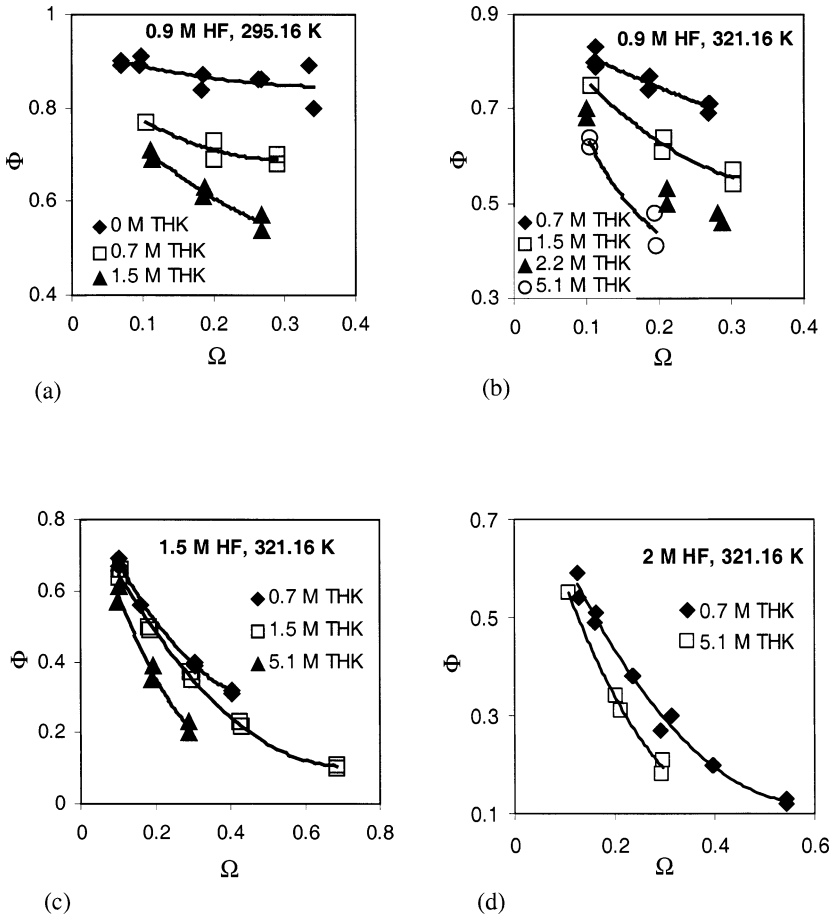

Figure 22. Effect of the thickener (THK) concentration at various fixed HF concentrations on the etched surface roughness as a function of the linear removal (etchant: HF + excess HNO_3 + H_3PO_4 + H_2O).[30] (Reproduced by permission of The Electrochemical Society, Inc.).

typical length scale of the wafer surface roughness measured in the semiconductor industry. Therefore, the application of the extrinsic bubbling in wafer etching is very common in the semiconductor industry.

Experiments: Effect of the Transport and the Kinetic Resistances. A series of experiments was performedusing the extrinsic nitrogen bubbling in the setup described in Figure 14a to establish effects of the mass-transport on improvement in the roughness of etched wafers. The experiments were conducted using various mixtures of HF and HNO_3 with and without the viscous thickener (H_3PO_4), at different temperatures, with wafers rotating at 6 rpm, at approximately 6×10^5 Pa upstream nitrogen pressure. Rough silicon wafers with very low gloss (0−5 gloss units) and high roughness ($0.2-0.3 \times 10^{-6}$ m) were etched in all experiments discussed below.

Effect of Thickeners. A mixture of HF and HNO_3 (and water) is not very viscous. Hence, the effective mass-transport resistance for such a mixture can be quite low. Addition of a chemically inert and thick viscous acid to this mixture increases the effective mass-transport resistance as a result of a decrease in the diffusivity of HF caused by an increase in the viscosity of the solution, that is,

$$\frac{\partial(\beta_{m,eff,HF})}{\partial\mu} > 0 \text{ and } \frac{\partial(\beta_{m,eff,HF})}{\partial C_{b,thk}} > 0 \qquad (41)$$

where μ is the viscosity (kg/m·s) of the etchant. Subscript "HF" refers to HF and "THK" refers to the thickener. Thus, $\beta_{m,eff,HF}/\beta_{r,eff,HF}$ increases with the thickener concentration (the effect of a change in the etchant viscosity is more on the effective mass-transport resistance than it is on the effective kinetic resistance). Since the addition of a thick viscous acid affects the polishing efficiency by predominantly decreasing the diffusivity of HF, the polishing efficiency must increase with increasing thickener concentration, in accordance with the limiting case 2 of the proposed pseudo two-phase model (Figure 12).

The polishing efficiency can be measured by the ratio of the decrease in roughness to the removal, $(-\Delta\Phi/\Omega)$. This ratio improves with the increasing concentration of the thickener. Figure 22 shows the effect of the thickener concentration on the roughness as a function of the removal. It is clearly observed that the thickener influences the mass-transport effects in etching and decreases the etched surface roughness.

Effect of The HF Concentration. Popularly used etchants contain excess nitric acid. In many cases, the molar ratio of HF:HNO_3 in the etching mixture varies from 1:10 to 1:5. Since nitric acid is in abundance, relative concentration of nitric acid does not vary appreciably during etching. Thus, HF becomes the rate-influencing reactant and the effective kinetic resistance ($\beta_{r,eff,HF}$) becomes a strong function of the interfacial concentration of HF. With increasing HF concentration, the effective kinetic resistance decreases if etching follows a kinetics of order greater than 1 with respect to HF or increases if the kinetics is of order less than 1. The effective mass transport resistance ($\beta_{m,eff,HF}$), however, is not a strong function of the HF concentration (it is assumed that the effective film thickness and the

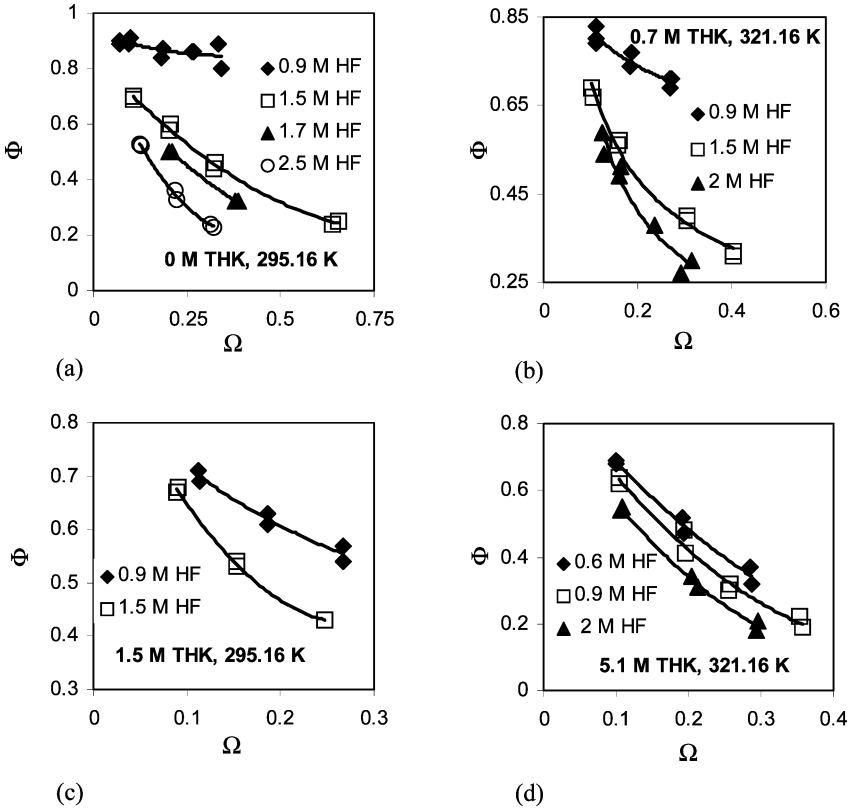

Figure 23. Effect of the HF concentration at various fixed thickener (THK) concentrations on the etched surface roughness as a function of the linear removal (etchant: HF + excess HNO_3 + H_3PO_4 + H_2O).[30] (Reproduced by permission of The Electrochemical Society, Inc.).

diffusivity do not vary appreciably with the concentration of a species if changes in the density and the viscosity of the mixture are negligible). Thus, with variation in the concentration of the key reactant, HF, the ratio of the effective mass-transport resistance to the effective kinetic resistance, $\beta_{m,eff,HF}/\beta_{r,eff,HF}$, can be varied. In accordance with the developed model, the following statement holds true:

$$\text{if } \frac{\partial\left(\frac{\beta_{m,eff,HF}}{\beta_{r,eff,HF}}\right)}{\partial C_{b,HF}} > 0, \text{ then } \frac{\partial \eta}{\partial C_{b,HF}} > 0$$
$$\text{if } \frac{\partial\left(\frac{\beta_{m,eff,HF}}{\beta_{r,eff,HF}}\right)}{\partial C_{b,HF}} < 0, \text{ then } \frac{\partial \eta}{\partial C_{b,HF}} < 0 \quad (42)$$

The polishing efficiency can be measured by the ratio of the change in the surface roughness to the removal, $(-\Delta\Phi/\Omega)$. Figure 23 shows the dependence of the etched surface roughness on the HF concentration, at different fixed thickener concentrations. Experimental data indicate that $(-\Delta\Phi/\Omega)$ increases with the increasing HF concentration. Hence, the effective kinetic resistance decreases, resulting in an increase in the polishing efficiency with the increasing HF concentration, in accordance with a kinetics of order greater than 1 with respect to HF. Figure 24 shows the improvement in the roughness of etched wafers for a fixed removal and, hence, the improvement in the polishing efficiency, with the increasing HF concentration. At higher HF concentrations, however, the etching rates are uncontrollably high and process control and runaway become a concern.

Effect of The Temperature. The temperature of an etchant, like the concentration of HF species, can affect

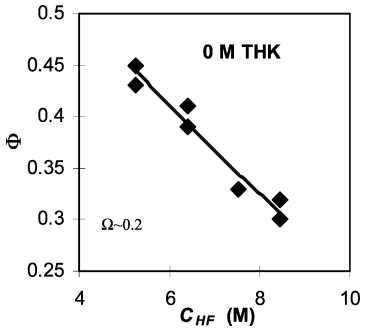

Figure 24. Surface roughness of etched wafers for a fixed removal as a function of increasing HF concentration (etchant: HF + excess HNO_3 + H_2O).[30] (Reproduced by permission of The Electrochemical Society, Inc.).

the effective kinetic resistance. It can also affect the effective mass-transport resistance. Typically, both the effective kinetic resistance and the effective mass-transport resistance decrease with an increase in the temperature. The former is predominantly the result of kinetics and the latter is a result of reduction in both the viscosity and the density of the etchant, which increases the diffusivities of all reagents, with increasing temperature. Therefore, the systems marked by highly temperature-sensitive transport parameters (compared to the kinetic parameters) show decreasing polishing efficiency with the increasing temperature, and the systems following highly temperature-sensitive kinetics show increasing polishing efficiency with the increasing temperature. The systems in which both the effective transport and the effective kinetic resistances vary comparably with the temperature show no incremental effect of the temperature on the polishing efficiency.

$$\frac{\partial\left(\frac{\beta_{m,eff,HF}}{\beta_{r,eff,HF}}\right)}{\partial T} < 0 \text{ and } \frac{\partial \eta}{\partial T} < 0$$

for highly temperature sensitive transport

$$\frac{\partial\left(\frac{\beta_{m,eff,HF}}{\beta_{r,eff,HF}}\right)}{\partial T} > 0 \text{ and } \frac{\partial \eta}{\partial T} > 0$$

for highly temperature sensitive kinetics (43)

$$\frac{\partial\left(\frac{\beta_{m,eff,HF}}{\beta_{r,eff,HF}}\right)}{\partial T} \approx 0 \text{ and } \frac{\partial \eta}{\partial T} \approx 0$$

for similar dependence of kinetics and transport on temperature

The dependence of these parameters on the temperature, however, can be different under different etching conditions. Figure 25 shows a system in which both the effective mass-transport resistance and the effective kinetic resistance vary comparably with the temperature.

A Final Note on Surface Polishing. The discussion in this section focused on the chemical surface polishing by etching. A generic pseudo two-phase model to describe the complex three-phase dynamics of etching was developed and applied to various real systems. Performing various experiments and analyzing the collected data provided insight into various aspects of etching. The next section focuses on the application of the developed etching model in describing defect decoration in monocrystalline silicon. The conclusions for both the sections (I and II) are listed in the end.

Section II: Acid-Based Etching in Defect Characterization

The silicon crystal grown by both Float Zone and Czochralski processes inherently contains many crystallographic imperfections. Dislocations primarily formed by thermomechanical stresses in the vicinity of the melt/crystal interface were the most common type of imperfections in the crystals grown prior to the 1950s. A major breakthrough by Dash allowed growth of dislocation-free crystals.[34,35] Various types of crystallographic imperfections popularly known as *microdefects*, however, were introduced in the absence of thermomechanically induced dislocations. The microdefects are primarily of two origins—*vacancy* and *self-interstitial*.[36] Vacancies are formed by a missing atom in the crystal lattice, and a self-interstitial is a silicon atom that is displaced from its normal lattice position. Both vacancies and self-interstitials, which are collectively known as the *point defects*, exist as solutes in the bulk silicon solvent. The solubility of point defects exponentially increases with the temperature.[1,36] As a segment of a growing crystal moves away from the melt/crystal interface, the temperature of the crystal segment decreases, allowing the gradual supersaturation of either vacancies or self-interstitials, depending on the crystal growth conditions.[36] In early crystals, sufficient surface area for *absorption* of the point defects was provided by the dislocation loops formed by the thermomechanical stress. In the absence of such surface area, however, both self-interstitials and vacancies homogeneously agglomerate to form precipitates, which are known as microdefects. One of the early reports of interstitial-related microdefects was made by Abe and co-workers, although the origin of these defects was not clearly known.[37] These defects were later termed *A-defects* and *B-defects* and were eventually identified as interstitial-related dislocation loops and three-dimensional interstitial agglomerates, respectively.[38−40] Among others, Roksnoer and van den Boom reported vacancy agglomerates, which were later termed *D-defects*.[41]

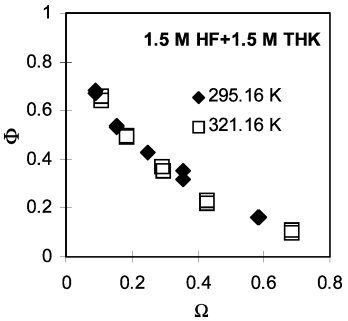

Figure 25. Effect of the etching temperature on the etched surface roughness (etchant: HF + excess HNO_3 + H_3PO_4 + H_2O).[30] (Reproduced by permission of The Electrochemical Society, Inc.).

Microdefect Decoration: A Brief History. The demand on quality of the silicon substrate becomes more stringent as the size of devices decreases in the current microelectronics industry. The size and the spatial distribution of both vacancy- and interstitial-type agglomerated microdefects play a critical role in device failure. Therefore, the sizes and the distribution of the microdefects define the quality of a silicon wafer. Device makers have varying wafer-quality requirements and the challenge of producing different types of silicon wafers to meet different device makers' specifications is on the wafer manufacturer. Identification and characterization of the microdefects forms a significant part of the research, development, and subsequent production of a silicon wafer of a required quality.

A popular method of microdefect characterization is chemical etching. Most popular etchants used in the microdefect decoration are mixtures of an oxidant (or a few oxidants), a chemical dissolving agent (generally, hydrofluoric acid), and diluents. Stress levels in the perfect silicon lattice are different from local stress levels at the microdefects. A class of etchants known as *microdefect-decorating etchants*, or simply, *decorating etchants*, shows sensitivity to this difference in the stress levels. The etching rates of the microdefects are different from the etching rates of the normal silicon or perfect silicon, in the presence of a decorating etchant. This differential etching creates the pits known as the *etch-pits* (or hillocks in rare cases) at the microdefect sites, which then can be identified under a microscope. Oxidants and diluents used in an etching mixture influence its microdefect-decorating capacity. The popular oxidants used are HNO_3, CrO_3, $K_2Cr_2O_7$, and $Cu(NO_3)_2$. Most common diluents are H_2O, CH_3COOH, and other acids. Sirtl and Adler, Secco d'Aragona, Schimmel, Jenkins, and Yang were among many others who successfully experimented with various compositions of oxidants, HF, and diluents to characterize the microdefects.[42−46] Schimmel compared performances of different acid etchants in defect decoration and gave a qualitative

explanation for the defect decoration based on differences in local etching rates.[44]

Forced precipitation of selective metal solutes on the microdefects can also accomplish microdefect decoration. Typically, metals precipitate as silicides. The technique involves saturation of silicon wafer with a metal impurity at a high temperature followed by rapid cooling to allow supersaturation of the impurity and its subsequent precipitation on the microdefects. Copper is the most frequently used impurity to decorate the microdefects in silicon wafers.[47] The copper decorated microdefects can be characterized by optical or infrared microscopy, transmission X-ray topography, or Lang XRT method.[47−49] Since the 1970s, considerable progress has been made in characterizing *copper precipitates*, which are recognized as Cu_3Si, and the method of copper precipitation for microdefect decoration has been very well established.[50,51]

In the past, the techniques of the copper precipitation and the decorating etching for microdefect characterization were not applied in conjunction with each other. The density of a copper precipitate is much lower than that of silicon. Therefore, growth of a copper precipitate generates compressive stresses in the surrounding area. These stresses are relieved by ejection of silicon lattice atoms as self-interstitials. New dislocations around the copper precipitate are formed by the ejected self-interstitials.[51] Subsequent copper precipitation can take place on these dislocations. This precipitate-influenced region, containing many copper precipitates and dislocations formed around a single microdefect, is identified as a *copper precipitate colony* or *copper colony*. Different precipitate colonies are formed by different metals. A copper precipitate colony is much larger in size than is the original microdefect.[51] After the copper precipitation, a *microdefect site* is identified by a much enlarged region occupied by the associated copper precipitate colony. Hence, the copper precipitation followed by a decorating etching accomplishes a more efficient characterization of the microdefects.[52]

In the current literature, there is an abundance of information on both the copper precipitation and the decorating etching. The difference between the etching rate of the microdefects and of the surrounding perfect silicon defines the basis of current understanding of the microdefect decoration by etching. Generally, this difference is attributed to the difference in the kinetics between the two regions. The kinetics, however, describes only the surface reactions. The generic theory of etching proposed in the previous section incorporates both the mass-transport and the kinetic effects and shows that the presence of the liquid-phase transport effects typically reduces the intensity of surface irregularities such as the roughness and resists formation of surface irregularities because of a *polishing effect*. Since the etch-pits formed by a decorating etchant are also surface irregularities, it can be argued that the presence of the significant mass-transport effects can affect the quality of microdefect decoration. The relative magnitude of the mass-transport time scale compared to that of the kinetic time scale is the key parameter that describes the quality of microdefect decoration. Kulkarni et al. developed a concise model that can relate the quality of microdefect decoration to both the mass-transport and the kinetic effects.[53] They also studied and quantified the quality of microdefect decoration by incorporating these effects and identified parameters

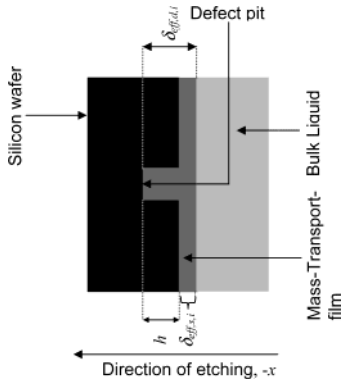

Figure 26. Phenomenological representation of the microdefect decoration by etching.[53] (Reproduced by permission of The Electrochemical Society, Inc.).

that determine the nature of an etchant as either polishing or decorating. The details of the study accomplished by Kulkarni et al. are discussed in this section of the paper.[53]

Procedure for Microdefect Decoration. Advantages of copper precipitation as well as decorating etching are combined by a hybrid decorating technique. The following steps are sequentially followed:

(1) Saturation of the silicon wafer with copper at a temperature above 800 °C.

(2) Rapid cooling of the silicon wafer to allow heterogeneous nucleation of copper on the microdefects and subsequent growth of copper precipitate colonies.

(3) Chemical surface polishing to clean the wafer surface.

(4) Decorating etching to decorate the copper precipitate colonies.

Decorating and Polishing Etching: Model. The pseudo two-phase model developed in the previous section is applied to describe the microdefect decoration in this section. Since only the effective resistances and the effective film thickness are used in the discussion of this section, the prefix "effective" is often dropped while addressing the effective parameters. The definition of all parameters used in this section remains consistent with the already defined parameters in the previous section. In this manner, both the chemical surface polishing and the microdefect decoration can be explained by one unifying theory.

Quantification of Microdefect Decoration. Microdefect decoration results because the etching rates (dissolution rates) of the copper precipitate colonies are higher than the etching rates of the surrounding perfect silicon. This work treats only the copper precipitate-enhanced microdefect decoration. Each copper precipitate colony represents a microdefect. Figure 26 shows a part of a silicon wafer with a microdefect-related etch-pit of depth h (m), covered by a liquid film of thickness $\delta_{\mathrm{eff,s},i}$ (m) on the surface and $\delta_{\mathrm{eff,d},i}$ (m) on the pit. The variable h represents a measure of the surface deformity. In the previous section, the surface deformity was measured by the average distance between peaks and valleys on a rough surface. In this section, the surface deformity of relevance is the etch-pit depth. Although etching takes place in all directions, for generic simplicity, let us assume effective etching to take place predominantly in the $-x$ direction. The rate of increase in the pit depth is given by the difference between the linear removal rate of the copper precipitate colony and that of the silicon surface:

$$\frac{dh}{dt} = u_d - u_s \tag{44}$$

where

$$u_d = \xi_{d,i} r_{d,i} \tag{45}$$

$$u_s = \xi_{s,i} r_{s,i} \tag{46}$$

where the subscript "d" denotes the copper precipitate colony and the etch-pit formed by it and "s" denotes the perfect silicon surface. The subscript "d" also denotes the pit after the complete dissolution of the copper precipitate colony. The maximum rate at which the pit depth can increase is given by

$$\left[\frac{dh}{dt}\right]_{max} = u_d \tag{47}$$

The *decorating efficiency* (I) can be defined as the ratio of the rate of increase in the pit depth to the maximum possible rate of increase in the pit depth.

$$I = \frac{\frac{dh}{dt}}{\left[\frac{dh}{dt}\right]_{max}} = 1 - \frac{\beta_{r,eff,d,i}}{\beta_{r,eff,s,i}}\left[\frac{1 + \frac{\beta_{m,eff,d,i}}{\beta_{r,eff,d,i}}}{1 + \frac{\beta_{m,eff,s,i}}{\beta_{r,eff,s,i}}}\right] = 1 - \frac{\xi_{s,i}}{\xi_{d,i}}\frac{R_{r,eff,d,i}}{R_{r,eff,s,i}}\left[\frac{1 + \frac{R_{m,eff,d,i}}{R_{r,eff,d,i}}}{1 + \frac{R_{m,eff,s,i}}{R_{r,eff,s,i}}}\right] \tag{48}$$

The *average decorating efficiency* is the integral average of the decorating efficiency during the pit growth.

$$I_{avg} = \frac{\int_{h_1}^{h_2}\left(\frac{dh}{dt}\Big/\left[\frac{dh}{dt}\right]_{max}\right)dh}{h_2 - h_1} \tag{49}$$

where the subscripts 1 and 2 indicate the pit depth at the onset and the end of decoration.

Equation 48 demonstrates the effect of the liquid-phase transport on the microdefect decoration. The microdefect decoration takes place only when the decorating efficiency is positive, and its quality is strongly influenced by the effective mass-transport resistance.

In the presence of a copper precipitate colony, the decorating efficiency remains positive and finite at a pit during decorating etching. No further increase in the pit depth is possible after the complete dissolution of the given copper precipitate colony at the pit, because the effective kinetic resistance at the pit and that at the surface are described by the same kinetics in the absence of a copper precipitate colony. In the absence of significant mass-transport effects, the geometry of the pit, however, is preserved throughout the decorating etching process, as the etching rate of the pit remains practically equal to the etching rate of the surface.

Quantification of Surface Polishing. The polishing efficiency has already been defined in the previous section in the context of the chemical surface polishing. The polishing efficiency is a measure of decrease in the local surface deformity and, hence, is defined in context of the nature of the local surface deformity. Polishing at a microdefect site or an etch-pit takes place when the etching rate of the etch-pit (more precisely, of the bottom of the etch-pit or valley) is lower than the etching rate on the surrounding planar areas. Thus, in the context of microdefect polishing, the polishing rate is defined as the rate of decrease in the distance between the bottom of the defect pit (etch-pit) and the perfect surface. This definition is analogous to the definition of the polishing rate with reference to the rate of decrease in the average distance between valleys and peaks on a rough surface, as defined in the context of reduction in the surface roughness. With reference to Figure 26, the polishing rate is defined as

$$-\frac{dh}{dt} = u_s - u_d \tag{50}$$

The maximum local polishing rate is achieved when the linear removal rate at the pit, u_d, is equal to zero:

$$\left[-\frac{dh}{dt}\right]_{max} = u_s \tag{51}$$

The *polishing efficiency* of any etchant at the microdefect site (or etch-pit) is defined as the rate of decrease in the pit depth to the maximum possible rate of decrease. It must be noted that the polishing efficiency at an etch-pit in the presence of an associated copper precipitate colony is lower than the polishing efficiency in its absence. In general, the polishing efficiency is given by the following equation:

$$\eta = \frac{-\frac{dh}{dt}}{\left[-\frac{dh}{dt}\right]_{max}} = 1 - \frac{\beta_{r,eff,s,i}}{\beta_{r,eff,d,i}}\left[\frac{1 + \frac{\beta_{m,eff,s,i}}{\beta_{r,eff,s,i}}}{1 + \frac{\beta_{m,eff,d,i}}{\beta_{r,eff,d,i}}}\right] = 1 - \frac{\xi_{d,i}}{\xi_{s,i}}\frac{R_{r,eff,s,i}}{R_{r,eff,d,i}}\left[\frac{1 + \frac{R_{m,eff,s,i}}{R_{r,eff,s,i}}}{1 + \frac{R_{m,eff,d,i}}{R_{r,eff,d,i}}}\right] \tag{52}$$

The average polishing efficiency of an etchant is the integral average of the polishing efficiency from h_1 to h_2:

$$\eta_{avg} = \frac{\int_{h_1}^{h_2}\left(-\frac{dh}{dt}\Big/\left[-\frac{dh}{dt}\right]_{max}\right)dh}{h_2 - h_1} \tag{53}$$

The polishing efficiency in the presence of the copper precipitate colonies must be negative for the microdefect decoration to take place. The polishing effect, however, may dominate in the presence of the liquid-phase transport effects. The microdefect decoration cannot proceed when the polishing efficiency in the presence of a copper precipitate colony is positive. The polishing

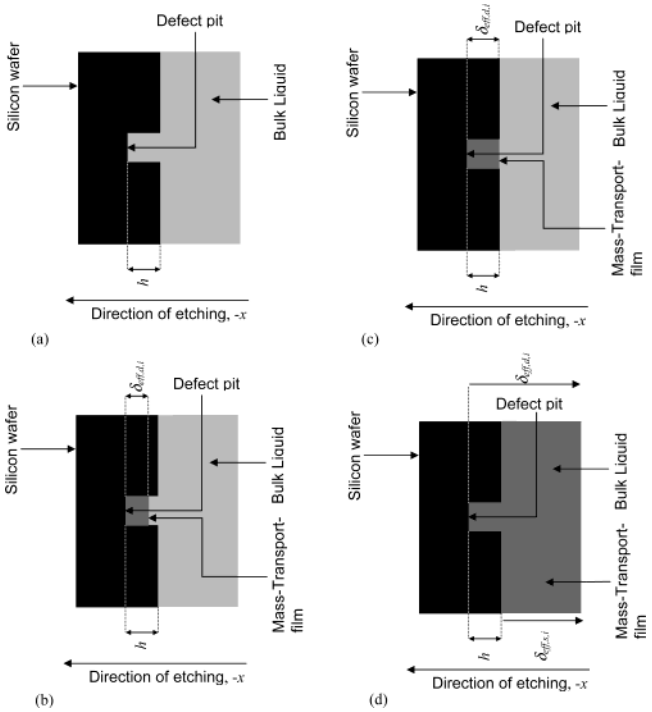

Figure 27. Phenomenological representation of the microdefect decoration (a) in the absence of the transport-film, (b) in the presence of a liquid cell in the etch-pit, (c) at $h = \delta_{\text{eff,d},i}$ and $\delta_{\text{eff,s},i} = 0$, (d) for the infinite effective mass-transport film thickness.[53] (Reproduced by permission of The Electrochemical Society, Inc.).

efficiency and the decorating efficiency have opposite signs except when both are equal to zero.

Microdefect Polishing and Normal Polishing. It is convenient to make a distinction between the *microdefect polishing* and the *normal polishing*. The polishing at the microdefect site or the microdefect polishing is resisted by the difference between the intrinsic etching kinetics of the native microdefect or the copper precipitate colony and that of the perfect silicon (i.e., $\beta_{\text{r,eff,d},i}$ and $\beta_{\text{r,eff,s},i}$ are described by different intrinsic kinetics). The *Normal polishing* takes place over a rough silicon surface or over the etch-pits in the absence of the microdefects or the copper precipitates, and is described by the same intrinsic kinetics. Thus, the effective intrinsic kinetics of the etched area remains the same for the normal polishing (i.e., $\beta_{\text{r,eff,d},i}$ and $\beta_{\text{r,eff,s},i}$ are described by the same intrinsic kinetics). An etchant can exhibit a negative polishing efficiency (positive decorating efficiency) in the presence of a copper precipitate colony and a positive polishing efficiency on the rough silicon surface or etch-pits, in the absence of such a colony or microdefect. Under such conditions, in the presence of the copper precipitates, small and shallow etch-pits are formed. These small pits, however, are erased after the copper precipitates are completely etched. Thus, an etch-pit can make a transition from decorating conditions to polishing conditions. This transition typically takes place upon the complete dissolution of the copper precipitate colony.

Microdefect Decoration and Surface Polishing: Analysis. The microdefects are decorated when the decorating efficiencies at the microdefect sites are positive. Surface irregularities including the microdefect related etch-pits are eventually erased if the normal polishing takes place. Equations 48 and 52 describe the generic effect of the mass-transport and the surface kinetics on any etching process. Insight into the role of the transport on the microdefect decoration, however, is better achieved by analyzing the following three limiting cases, each representing a popular industrial practice. For precipitate-aided decorating etching, typically $\beta_{\text{r,eff,d},i}/\beta_{\text{r,eff,s},i}$ is less than 1. The following discussion focuses on this case. The argument, however, can be extended to all generic conditions.

Limiting Case 1: Varying Effective Transport-Film Thickness. The effective mass-transport time scale and the effective mass-transport resistance each increase with increasing thickness of the effective transport film. The etchant composition and the hydrodynamic conditions in the etching reactor influence the thickness of this film. As the mixing intensity in a reactor increases, the effective mass-transport film thickness decreases.[32,33] Consider a hypothetical scenario shown in Figure 27. The film thickness is negligible at an extremely high mixing intensity in the etching reactor, as shown in Figure 27a. The etching is kinetically controlled, the decorating efficiency at the microdefect site (etch-pit) is at its highest (maximum) value, and the polishing efficiency at the site is at its lowest (minimum) value:

$$\lim_{\beta_{\text{m,eff,s},i}\to 0,\beta_{\text{m,eff,d},i}\to 0} I = 1 - \frac{\xi_{\text{s},i}}{\xi_{\text{d},i}}\frac{R_{\text{r,eff,d},i}}{R_{\text{r,eff,s},i}} = 1 - \frac{\beta_{\text{r,eff,d},i}}{\beta_{\text{r,eff,s},i}} \quad (54)$$

$$\lim_{\beta_{\text{m,eff,s},i}\to 0,\beta_{\text{m,eff,d},i}\to 0} \eta = 1 - \frac{\xi_{\text{d},i}}{\xi_{\text{s},i}}\frac{R_{\text{r,eff,s},i}}{R_{\text{r,eff,d},i}} = 1 - \frac{\beta_{\text{r,eff,s},i}}{\beta_{\text{r,eff,d},i}} \quad (55)$$

Liquid cells in the shallow etch-pits can develop as the hydrodynamic conditions in the reactor change, as shown in Figure 27b. These cells can be represented as an effective film that covers part of the pit. The decorating and the polishing efficiencies at the etch-pit at the microdefect site, under this condition, are given by

$$I = 1 - \frac{\xi_{\text{s},i}}{\xi_{\text{d},i}}\frac{R_{\text{r,eff,d},i}}{R_{\text{r,eff,s},i}}\left[1 + \frac{R_{\text{m,eff,d},i}}{R_{\text{r,eff,s},i}}\right] = 1 - \frac{\beta_{\text{r,eff,d},i}}{\beta_{\text{r,eff,s},i}}\left[1 + \frac{\beta_{\text{m,eff,d},i}}{\beta_{\text{r,eff,d},i}}\right] \quad (56)$$

$$\eta = 1 - \frac{\xi_{\text{d},i}}{\xi_{\text{s},i}}\frac{R_{\text{r,eff,s},i}}{R_{\text{r,eff,d},i}}\left[\frac{1}{1 + \frac{R_{\text{m,eff,d},i}}{R_{\text{r,eff,d},i}}}\right] = 1 - \frac{\beta_{\text{r,eff,s},i}}{\beta_{\text{r,eff,d},i}}\left[\frac{1}{1 + \frac{\beta_{\text{m,eff,d},i}}{\beta_{\text{r,eff,d},i}}}\right] \quad (57)$$

Equation 56 indicates that as the transport effects in the shallow pit increase, the decorating efficiency decreases. As the size of these liquid cells gradually increases, the decorating efficiency decreases and becomes zero when the condition

$$\beta_{\text{r,eff,d},i} + \beta_{\text{m,eff,d},i} - \beta_{\text{r,eff,s},i} = 0 \text{ and } \beta_{\text{m,eff,s},i} = 0 \quad (58)$$

is met. Equation 58 indicates the *crossover limit*. The crossover happens when the sum of the effective kinetic and the effective transport resistances at the pit equals the sum of the effective kinetic and the effective mass-transport resistances on the perfect surface. Beyond this limit, in the absence of the effective mass-transport resistance on the surface (i.e., for $\beta_{\text{m,eff,s},i} = 0$), an

increase in the effective mass-transport resistance at the shallow pit changes the etching condition from decorating to polishing.

A shift in the etchant behavior is observed when the effective surface mass-transport resistance becomes finite (nonzero). The threshold of this shift is determined by the equality of the effective mass-transport film thickness on the pit and the pit depth ($\delta_{\mathrm{eff,d},i} = h$) when the surface film thickness is still zero ($\delta_{\mathrm{eff,s},i} = 0$). At this shift, the critical values of the decorating efficiency and the polishing efficiency (Figure 27c) are still given by eqs 56 and 57, respectively. When both the wafer surface and the pit are covered by the transport film as shown in Figure 26, both the decorating efficiency and the polishing efficiency at the microdefect site are given by eqs 48 and 52, respectively. As the film thickness approaches infinity (Figure 27d), the decorating efficiency approaches an asymptotic value given by eq 59, and the polishing efficiency approaches an asymptotic value given by eq 60.

$$\lim_{\delta_{\mathrm{eff,d},i}\to\infty,\delta_{\mathrm{eff,s},i}\to\infty} I = 1 - \frac{\xi_{\mathrm{s},i}}{\xi_{\mathrm{d},i}}\frac{D_{\mathrm{eff,s},i}}{D_{\mathrm{eff,d},i}} \tag{59}$$

$$\lim_{\delta_{\mathrm{eff,d},i}\to\infty,\delta_{\mathrm{eff,s},i}\to\infty} \eta = 1 - \frac{\xi_{\mathrm{d},i}}{\xi_{\mathrm{s},i}}\frac{D_{\mathrm{eff,d},i}}{D_{\mathrm{eff,s},i}} \tag{60}$$

The marginal difference between the effective diffusivity on the etch-pit and the effective diffusivity on the surface arises as a result of the variation in the local bubble-related dynamics. The ratio $D_{\mathrm{eff,d},i}/D_{\mathrm{eff,s},i}$, however, is approximately equal to unity in most cases. A graph of the decorating efficiency (I) versus the ratio of the effective mass-transport resistance to the effective kinetic resistance ($\beta_{\mathrm{m,eff,d},i}/\beta_{\mathrm{r,eff,d},i}$) illustrates the behavior of an etchant as a function of the mass-transport and the kinetic effects at the microdefect site. Figure 28a shows a family of curves on this graph for a fixed pit depth and $\xi_{\mathrm{d},i}/\xi_{\mathrm{s},i} = 1$. Each curve on this graph is an *isokinetic line* representing a fixed ratio of the effective kinetic resistance at the etch-pit at the microdefect site to the effective kinetic resistance at the surface, $\beta_{\mathrm{r,eff,d},i}/\beta_{\mathrm{r,eff,s},i}$. For a given etchant, the locus of the decorating efficiency as a function of $\beta_{\mathrm{m,eff,d},i}/\beta_{\mathrm{r,eff,d},i}$ does not necessarily represent a fixed $\beta_{\mathrm{r,eff,d},i}/\beta_{\mathrm{r,eff,s},i}$ and, hence, does not necessarily represent an isokinetic line. A given point on that locus, however, lies on some isokinetic line. Thus, this graph can map all etchants. As $\beta_{\mathrm{r,eff,d},i}/\beta_{\mathrm{r,eff,s},i}$ increases, the kinetic tendency toward microdefect decoration, typically, decreases.

The ratio of the cumulative effects of the reaction stoichiometry and the density of the copper colony to those of the surrounding silicon is represented by the parameter $\xi_{\mathrm{d},i}/\xi_{\mathrm{s},i}$. For a fixed $R_{\mathrm{r,eff,d},i}/R_{\mathrm{r,eff,s},i}$, the decorating efficiency increases with increasing $\xi_{\mathrm{d},i}/\xi_{\mathrm{s},i}$. Figure 28b shows the dependence of the decorating efficiency on $\beta_{\mathrm{m,eff,d},i}/\beta_{\mathrm{r,eff,d},i}$ at the microdefect site, for different $\xi_{\mathrm{d},i}/\xi_{\mathrm{s},i}$, at a fixed pit depth and $R_{\mathrm{r,eff,d},i}/R_{\mathrm{r,eff,s},i}$. Each line on this graph represents a constant $\xi_{\mathrm{d},i}/\xi_{\mathrm{s},i}$.

The polishing behavior of any etchant is described on a graph of the microdefect-site polishing efficiency versus $\beta_{\mathrm{m,eff,d},i}/\beta_{\mathrm{r,eff,d},i}$, for a given pit depth (Figure 29a). The polishing capacity and the microdefect-decorating capacity exhibit an inverse relationship with each other. The microdefect-polishing tendency increases, typically, with increasing $\beta_{\mathrm{r,eff,d},i}/\beta_{\mathrm{r,eff,s},i}$. Figure 29a shows the isokinetic lines when $\xi_{\mathrm{d},i}/\xi_{\mathrm{s},i}$ is unity. For each $\xi_{\mathrm{d},i}/\xi_{\mathrm{s},i}$,

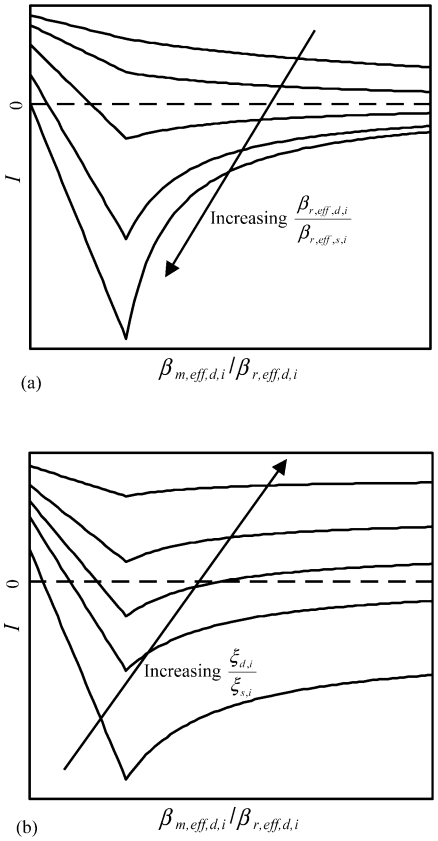

Figure 28. Effect of the effective mass-transport film thickness on the decorating efficiency at a microdefect site for a given pit depth and (a) a given $\xi_{\mathrm{d},i}/\xi_{\mathrm{s},i}$, (b) a given $R_{\mathrm{r,eff,d},i}/R_{\mathrm{r,eff,s},i}$.[53] (Reproduced by permission of The Electrochemical Society, Inc.).

there is a family of isokinetic lines. Figure 29b shows various constant $\xi_{\mathrm{d},i}/\xi_{\mathrm{s},i}$ lines for a fixed $R_{\mathrm{r,eff,d},i}/R_{\mathrm{r,eff,s},i}$ and for a given pit depth. The polishing efficiency decreases with increasing $\xi_{\mathrm{d},i}/\xi_{\mathrm{s},i}$.

Limiting Case 2: Varying Effective Diffusivity. The effective mass-transport time scale decreases with increasing effective diffusivity. Thus, for a fixed transport-film thickness, both the polishing efficiency and the decorating efficiency at the microdefect site are affected by the effective diffusivities of reactants. Consider the hypothetical scenario shown in Figure 30. The case for the infinite effective diffusivity is depicted by Figure 30a. The thickness of the effective mass-transport film is irrelevant when the effective diffusivity is infinite, as the effective mass-transport resistance is zero. Under these conditions, the decorating efficiency is at its highest (maximum) value, and the polishing efficiency is at its lowest (minimum) value. These efficiencies are quantified by eqs 54 and 55, respectively. When the effective diffusivity of the key reactant decreases (Figure 30b), the decorating efficiency decreases and the polishing efficiency increases. The decorating and the polishing efficiencies are quantified by eqs 48 and 52, respectively, under these conditions. As the effective diffusivity of the key reactant further decreases, the crossover occurs when the sum of the effective kinetic and the effective transport resistances at the etch-pit at the microdefect site equals the sum of the effective kinetic and the effective transport resistances on the perfect silicon surface.

$$\beta_{\mathrm{r,eff,d},i} + \beta_{\mathrm{m,eff,d},i} - (\beta_{\mathrm{r,eff,s},i} + \beta_{\mathrm{m,eff,s},i}) = 0 \tag{61}$$

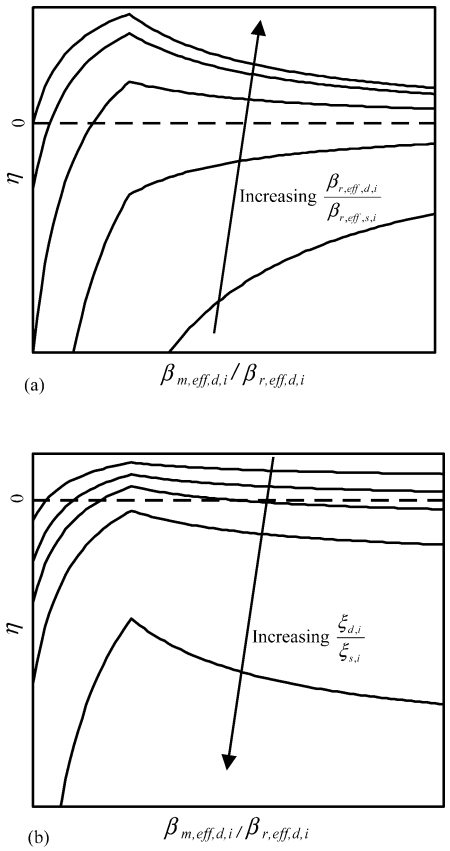

Figure 29. Effect of the effective mass-transport film thickness on the polishing efficiency at a microdefect site for a given pit depth and (a) a given $\xi_{d,i}/\xi_{s,i}$, (b) a given $R_{r,eff,d,i}/R_{r,eff,s,i}$[53] (Reproduced by permission of The Electrochemical Society, Inc.).

As the effective diffusivity approaches zero, the decorating and the microdefect-polishing efficiencies tend to the non-zero asymptotic values described by eqs 62 and 63, respectively:

$$\lim_{D_{eff,d,i}\to 0, D_{eff,s,i}\to 0} I = 1 - \frac{\xi_{s,i}}{\xi_{d,i}}\left(\frac{h}{\delta_{eff,s,i}} + 1\right) \qquad (62)$$

$$\lim_{D_{eff,d,i}\to 0, D_{eff,s,i}\to 0} \eta = 1 - \frac{\xi_{d,i}}{\xi_{s,i}}\frac{\delta_{eff,s,i}}{\delta_{eff,s,i} + h} \qquad (63)$$

It is quite interesting to note that the asymptotic value of the decorating efficiency at the etch-pit at the microdefect site is a constant negative value and the asymptotic value of the polishing efficiency at the site is a constant positive value, for $\xi_{d,i}/\xi_{s,i} = 1$. Thus, when the thickness of the effective transport film is finite, an increase in the effective transport resistance invariably improves the polishing quality and deteriorates the decorating capacity of an etchant.

A graph of the decorating efficiency (I) versus the ratio of the effective mass-transport resistance to the effective kinetic resistance ($\beta_{m,eff,d,i}/\beta_{r,eff,d,i}$) illustrates the effects of the transport and the kinetics on the microdefect decoration. The isokinetic lines on this graph for a fixed pit depth and $\xi_{d,i}/\xi_{s,i} = 1$ are shown in Figure 31a. As discussed earlier, an isokinetic line represents a fixed effective kinetic condition, ($\beta_{r,eff,d,i}/\beta_{r,eff,s,i}$). The decorating efficiency decreases with increasing $\beta_{r,eff,d,i}/\beta_{r,eff,s,i}$. The effect of $\xi_{d,i}/\xi_{s,i}$ at a given $R_{r,eff,d,i}/R_{r,eff,s,i}$ and pit depth is shown in Figure 31b, in terms of various constant $\xi_{d,i}/\xi_{s,i}$ lines. Here, the decorating efficiency increases with increasing $\xi_{d,i}/\xi_{s,i}$.

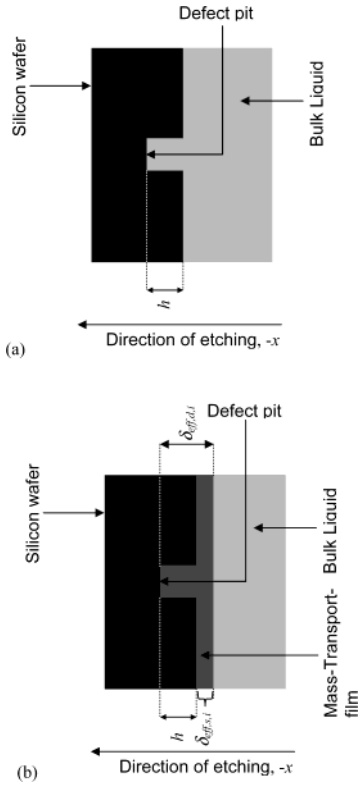

Figure 30. Phenomenological representation of the microdefect decoration for a finite mass-transport film thickness and (a) the infinite effective diffusivity or the infinite effective kinetic resistance and (b) a finite effective diffusivity or a finite effective kinetic resistance.[53] (Reproduced by permission of The Electrochemical Society, Inc.).

Figure 32a shows the polishing behavior when $\xi_{d,i}/\xi_{s,i}$ is unity. The polishing efficiency at an etch-pit at a microdefect site increases with increasing $\beta_{m,eff,d,i}/\beta_{r,eff,d,i}$ and reaches an asymptotic positive value. It is also illustrated that the polishing efficiency increases with increasing $\beta_{r,eff,d,i}/\beta_{r,eff,s,i}$. The effect of $\xi_{d,i}/\xi_{s,i}$ on the polishing efficiency is shown in Figure 32b. The polishing efficiency decreases as $\xi_{d,i}/\xi_{s,i}$ increases.

Limiting Case 3: Varying Effective Kinetic Resistance. Effects of variations in the effective kinetic resistance and the effective diffusivity are similar in nature, for a fixed effective mass-transport film thickness. At the infinite effective kinetic resistance, the mass-transport effects are negligible (Figure 30a). The decorating efficiency is at its maximum value (eq 54) and the polishing efficiency (eq 55) is at its minimum value. As the effective kinetic resistance decreases, the mass-transport effects set in (Figure 30b), and the decorating efficiency (described by eq 48) decreases while the polishing efficiency (described by eq 52) increases. The crossover limit is given by eq 61. The asymptotic values of the decorating efficiency and the polishing efficiency are given by

$$\lim_{\beta_{r,eff,d,i}\to 0, \beta_{r,eff,s,i}\to 0} I = 1 - \frac{\xi_{s,i}}{\xi_{d,i}}\left(\frac{h}{\delta_{eff,s,i}} + 1\right)\frac{D_{eff,s,i}}{D_{eff,d,i}} \qquad (64)$$

$$\lim_{\beta_{r,eff,d,i}\to 0, \beta_{r,eff,s,i}\to 0} \eta = 1 - \frac{\xi_{d,i}}{\xi_{s,i}}\frac{\delta_{eff,s,i}}{\delta_{eff,s,i} + h}\frac{D_{eff,d,i}}{D_{eff,s,i}} \qquad (65)$$

$D_{eff,s,i}/D_{eff,d,i}$ is, typically, very close to unity and, thus, can be ignored. The system dynamics is captured very well on the graphs of the decorating efficiency versus

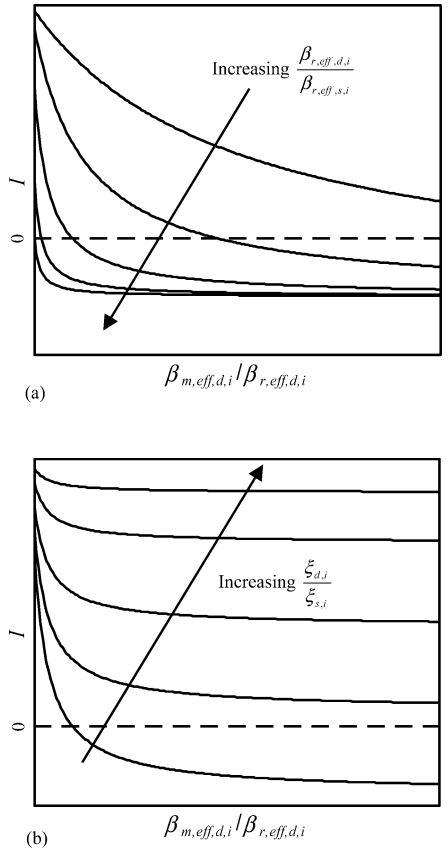

Figure 31. Effect of the effective diffusivity or the effective kinetic resistance on the decorating efficiency at a microdefect site for a given pit depth, a given mass-transport film thickness, and (a) a given $\xi_{d,i}/\xi_{s,i}$ and (b) a given $R_{r,eff,d,i}/R_{r,eff,s,i}$.[53] (Reproduced by permission of The Electrochemical Society, Inc.).

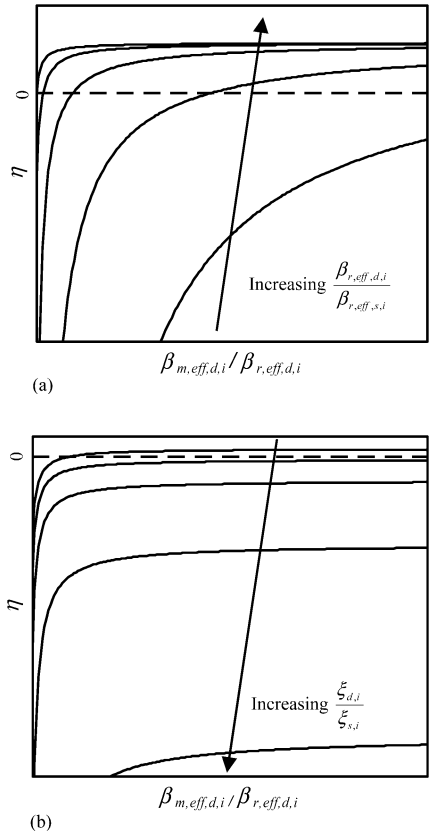

Figure 32. Effect of the effective diffusivity or the effective kinetic resistance on the polishing efficiency at a microdefect site for a given pit depth, a given mass-transport film thickness, and (a) a given $\xi_{d,i}/\xi_{s,i}$ and (b) a given $R_{r,eff,d,i}/R_{r,eff,s,i}$.[53] (Reproduced by permission of The Electrochemical Society, Inc.).

$\beta_{m,eff,d,i}/\beta_{r,eff,d,i}$ (Figure 31) and the polishing efficiency versus $\beta_{m,eff,d,i}/\beta_{r,eff,d,i}$ (Figure 32).

Auto-inhibiting Decoration. In the presence of the mass-transport effects, a weak microdefect decoration can be auto-inhibiting in nature. The etch-pit depth (h) at a microdefect site increases for a positive local decorating efficiency. The effective mass-transport resistance on the pit, however, increases as the pit depth increases, while the effective mass-transport resistance on the perfect silicon surface remains relatively unchanged. Thus, the decorating efficiency gradually decreases with increasing pit depth. This auto-inhibition is explained by eqs 48 and 52, which can be rewritten as

$$I = 1 - \frac{\beta_{r,eff,d,i}}{\beta_{r,eff,s,i}}\left[\frac{1 + \frac{(h + \delta_{eff,s,i})}{D_{eff,d,i}}\frac{1}{\xi_{d,i}\beta_{r,eff,d,i}}}{1 + \frac{\delta_{eff,s,i}}{D_{eff,s,i}}\frac{1}{\xi_{s,i}\beta_{r,eff,s,i}}}\right] \quad (66)$$

$$\eta = 1 - \frac{\beta_{r,eff,s,i}}{\beta_{r,eff,d,i}}\left[\frac{1 + \frac{\delta_{eff,s,i}}{D_{eff,s,i}}\frac{1}{\xi_{s,i}\beta_{r,eff,s,i}}}{1 + \frac{(h + \delta_{eff,s,i})}{D_{eff,d,i}}\frac{1}{\xi_{d,i}\beta_{r,eff,d,i}}}\right] \quad (67)$$

Therefore, the intensity of the microdefect decoration decreases as the decoration proceeds. The local decorating efficiency at the etch-pit can become zero even before the complete dissolution of the copper precipitate colony, for an etchant sensitive to an increase in the effective film thickness. The pit depth is at its maximum when the decorating efficiency becomes zero. This condition is quantified by eq 68:

$$h_{max} = \xi_{d,i}D_{eff,d,i}(\beta_{r,eff,s,i} - \beta_{r,eff,d,i}) - \delta_{eff,s,i}\left(1 - \frac{\xi_{d,i}}{\xi_{s,i}}\frac{D_{eff,d,i}}{D_{eff,s,i}}\right) \quad (68)$$

where the subscript "max" denotes the maximum value. As the effective diffusivity, $D_{eff,i}$, decreases, the auto-inhibiting capacity increases. The auto-inhibition can be described on a graph of the local decorating efficiency versus the pit depth, as shown in Figure 33a. The auto-inhibition shows an inverse relationship with the effective diffusivity. The etchants with higher effective mass-transport resistances show greater tendencies toward the auto-inhibition. In other words, the microdefect decoration is very poor when the transport effects are dominant. The effect of the mass-transport on the auto-inhibition on a h_{max} versus $\beta_{m,eff,s,i}$ graph is shown in Figure 33b.

Theoretical Classification of Etchants. The decorating and the polishing capacities of various etchants for the precipitate-enhanced microdefects are discussed in the following subsections. This discussion, however, can be extended to native microdefects in the absence of any impurity precipitation. In this study, the microdefect decoration was accomplished using the copper precipitation. Hence, the terms microdefect decoration and microdefect polishing generally refer to the decora-

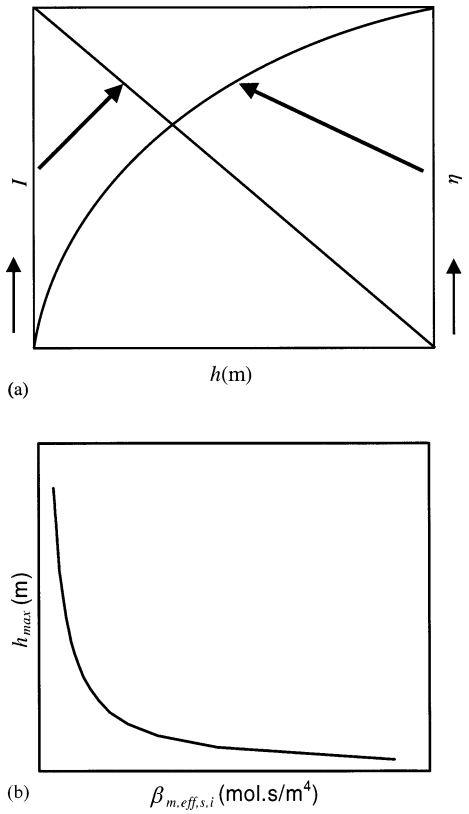

Figure 33. Auto-inhibition of the microdefect decoration (a) with increasing pit depth, (b) as a function of the effective mass-transport resistance.[53] (Reproduced by permission of The Electrochemical Society, Inc.).

tion and the polishing in the presence of the copper precipitate colonies, respectively.

An etchant can be identified based on a quantitative analysis of its polishing and decorating capacities. Etchants can be classified into four categories: *neutral*, *decorating*, *microdefect polishing*, and *normal polishing*. A neutral etchant shows negligible decorating and polishing efficiencies in the presence of a precipitate colony. A decorating etchant shows a positive decorating efficiency in the presence of a precipitate colony. A microdefect-polishing etchant shows a positive polishing efficiency at a microdefect site in the presence of a precipitate colony. A microdefect-polishing etchant completely inhibits the microdefect decoration. A normal-polishing etchant shows a positive decorating efficiency at a site in the presence of a precipitate colony and a positive polishing efficiency at the same site upon the complete dissolution of the colony. This happens because the ratio of the effective kinetic resistance at the microdefect site to that on the perfect silicon surface ($\beta_{r,eff,d,i}/\beta_{r,eff,s,i}$) is greater in the absence of the precipitate colonies than that in the presence of these colonies. Thus, a normal-polishing etchant can weakly decorate the microdefects by creating etch-pits in the presence of the precipitate colonies and subsequently polish and erase these etch-pits after the complete dissolution of the colonies. In a copper-precipitated wafer, it is normal to have local variation of the polishing efficiency of an etchant—positive at the perfect region away from the copper precipitate colonies and negative at the microdefect sites in the presence of the colonies. Both the normal-polishing and the microdefect-polishing etchants decrease surface irregularities such as the surface roughness in the absence of the copper precipitate

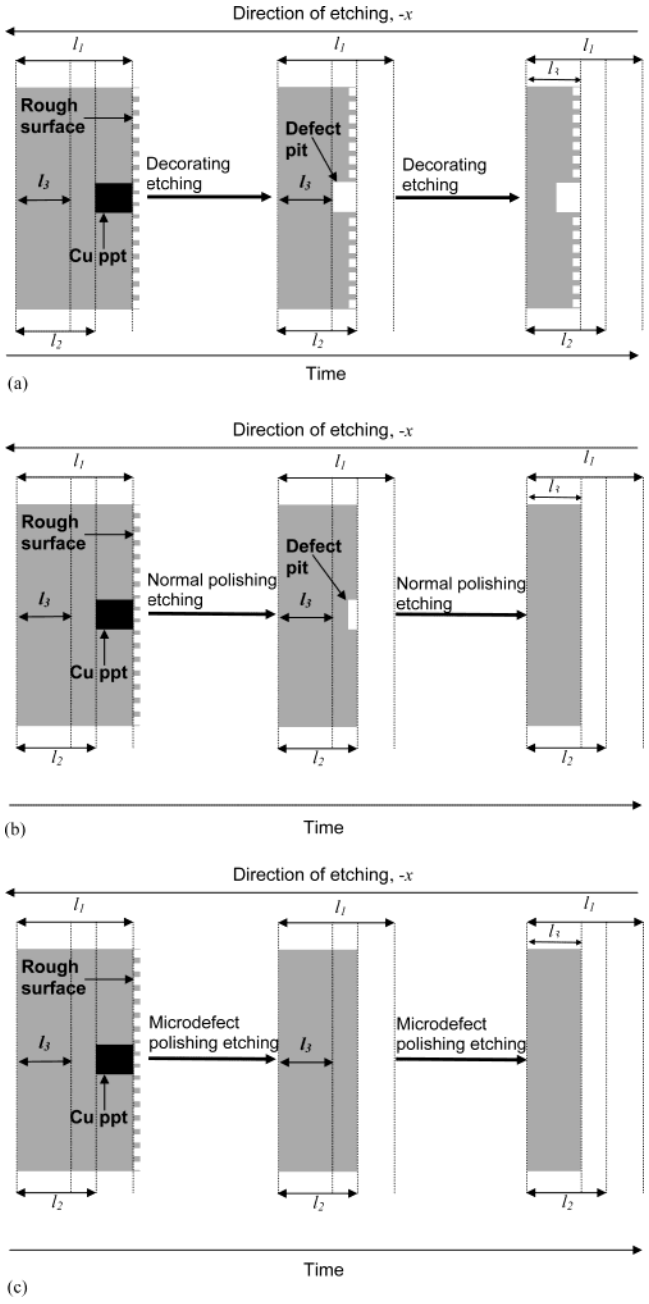

Figure 34. Schematic representation of (a) the microdefect decoration by a decorating etchant, (b) a weak microdefect decoration and subsequent erasure by a normal polishing etchant, (c) microdefect erasure by a microdefect-polishing etchant.[53] (Reproduced by permission of The Electrochemical Society, Inc.).

colonies, whereas neither the neutral nor the decorating etchants can do so. The working models for the decorating, normal-polishing, and microdefect-polishing etchants are described in Figure 34.

The group of *polishing etchants* consists of both the microdefect-polishing and the normal-polishing etchants. A polishing etchant is sensitive to hydrodynamic conditions in the etching reactor, whereas a decorating etchant is relatively independent of the hydrodynamic conditions. In a mass-transport-influenced reactor, the effective transport-film thickness decreases with increasing mixing intensity.[33,34] Thus, the etching rate increases with the mixing intensity under polishing conditions as a result of the decreasing effective mass-transport film thickness. Conversely, under decorating conditions, the etching rate does not show a significant

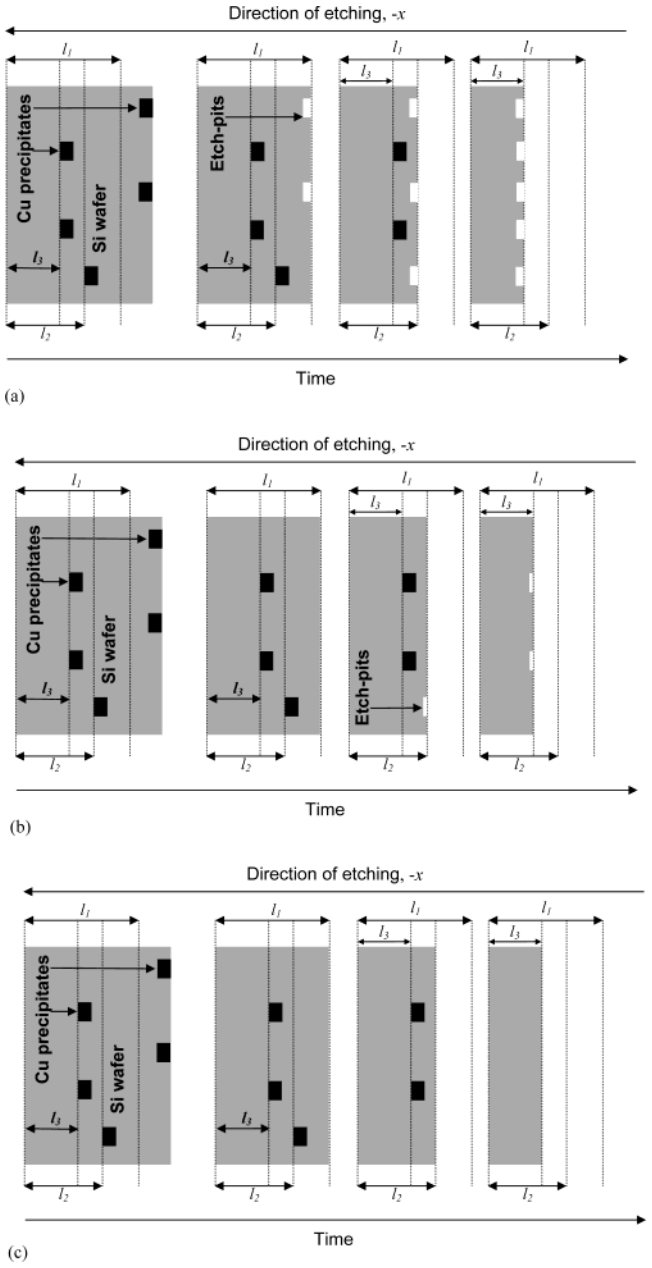

Figure 35. Global picture of (a) the microdefect decoration by a decorating etchant, (b) a weak microdefect decoration and subsequent erasure by a normal polishing etchant, (c) microdefect erasure by a microdefect-polishing etchant.[53] (Reproduced by permission of The Electrochemical Society, Inc.).

change with the mixing intensity because the effective mass-transport film is practically absent. It must be noted, however, that the neutral etchants can also show insensitivity to the hydrodynamic conditions. Only those etchants that show a difference between the effective microdefect kinetics and the effective surface kinetics and are relatively independent of the hydrodynamic conditions are decorating. Therefore, the etchants that are insensitive to the mixing intensity can be defined as *potentially decorating*, at best, rather than as decorating.

Thus, etchants can be divided into two broader categories: potentially decorating and polishing. The potentially decorating etchants include both the decorating etchants and the neutral etchants. Both the normal-polishing and the microdefect-polishing etchants are the polishing etchants.

Table 1. Components of Various Popular Etchants[53] (Reproduced by Permission of The Electrochemical Society, Inc.)

etchant	components	classification
MAE[a]	HNO_3, HF, CH_3COOH, H_2O	polishing
HF + HNO_3[a]	HNO_3, HF, H_2O	polishing
HF + HNO_3 + H_3PO_4[a]	HNO_3, HF, H_3PO_4, H_2O	polishing
Secco[a]	$K_2Cr_2O_7$, HF, H_2O	decorating
Wright[a]	$K_2Cr_2O_7$, HNO_3, $Cu(NO_3)_2$, HF, CH_3COOH, H_2O	decorating

[a] Actual concentrations of the components may be different from what is reported in the literature.

A Global Picture of Microdefect Decoration. The total number of etch-pits on a decorated silicon wafer surface is influenced by the microdefect density and the total removal. The global mechanism of the microdefect decoration in the presence of a decorating etchant is shown in Figure 35a. The copper precipitate colonies are of finite dimensions. A copper precipitate colony dissolves into the etching mixture by creating a pit, which becomes an irregular perfect (normal) silicon site upon the complete dissolution of the colony. The pits formed on the surface maintain their identity throughout the etching process since the decorating etchant lacks the surface polishing quality, while the interior copper precipitate colonies are exposed as the new pits. Thus, the apparent surface density of the pits is a function of the true microdefect density and the total linear removal by the decorating etchant.

A normal-polishing etchant weakly decorates the microdefects by creating the etch-pits and eventually erasing them. Thus, the microdefect decoration by a normal-polishing etchant is sparse and very weak. In the presence of a normal-polishing etchant, only the microdefect sites exposed at the end of the etching period appear as shallow pits. Figure 35b shows a weak microdefect decoration by a normal-polishing etchant. A microdefect-polishing etchant does not allow etch-pit formation, and hence, there is no defect decoration (Figure 35c).

Experimental Classification of Etchants. The proposed theory was experimentally verified. A group of decorating and polishing etchants was chosen. The components of the chosen etchants are listed in Table 1. It must be noted that the actual concentrations of the components play a very important role in defining the nature of an etchant. In this study, however, it is not necessary to reveal the actual concentrations of the components. The potentially decorating and the polishing etchants show distinct hydrodynamic responses according to the theory of etching discussed in this study. The classification of the chosen etchants into two groups, *namely*, potentially decorating and polishing, is accomplished by doing two sets of experiments.

First, in the experimental assembly shown in Figure 36a, precipitate-free silicon pieces were etched in a given etchant. The assembly includes a mechanism that allows the etching of silicon pieces at different rotation rates. The mixing intensity in the etching tank can be reasonably measured by the rotation rate. With use of this experimental assembly, the etching rate versus the rotation rate data were collected for all etchants (Figure 36b). MAE, HF + HNO_3, and HF + HNO_3 + H_3PO_4 show a significant increase in the etching rates with increasing mixing intensity, whereas Secco and Wright etchants show a weak dependence on the mixing intensity. At this stage, it can be concluded that MAE,

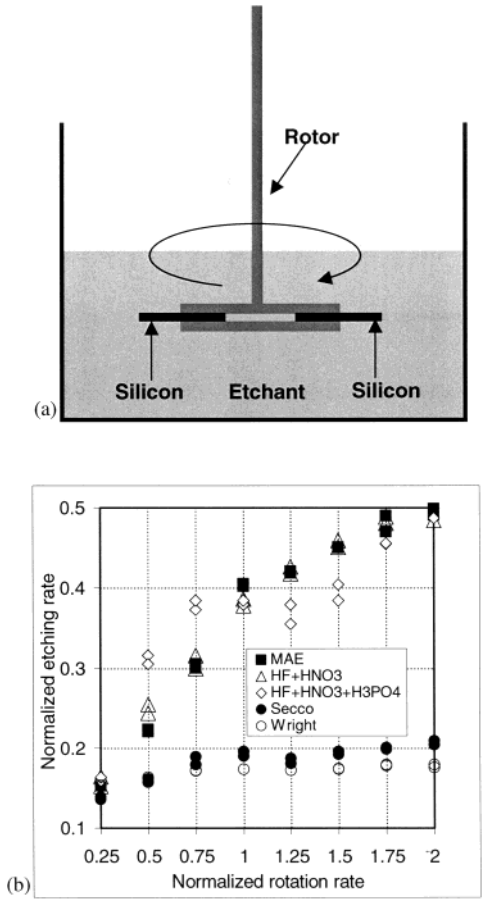

Figure 36. (a) An experimental assembly to etch silicon at different controlled mixing intensities. (b) Dependence of the etching rate as a function of the reactor mixing intensity for various popular etchants.[53] (Reproduced by permission of The Electrochemical Society, Inc.).

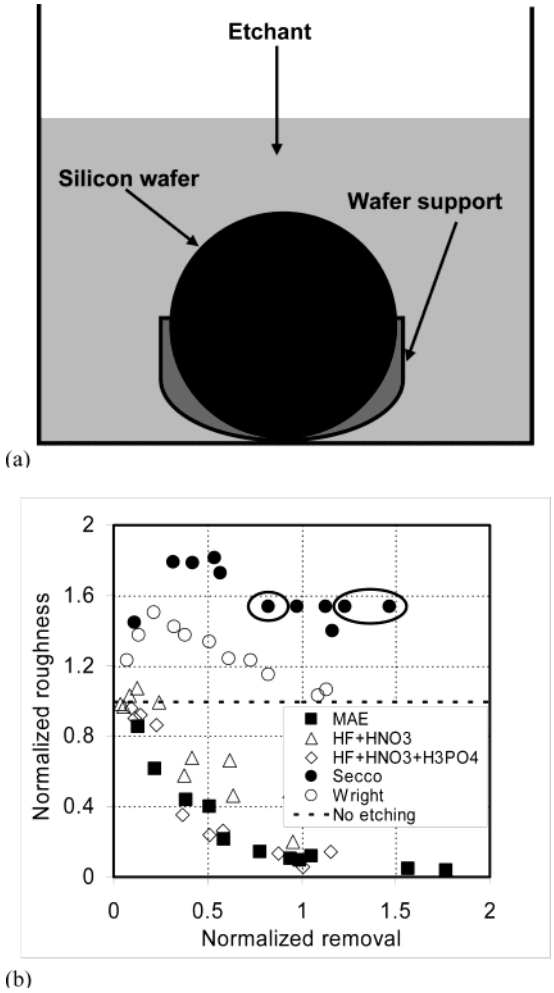

Figure 37. (a) An experimental assembly to etch silicon wafers in a given etchant. (b) Polishing effect of various popular etchants.[53] (Reproduced by permission of The Electrochemical Society, Inc.).

$HF + HNO_3$, and $HF + HNO_3 + H_3PO_4$ are polishing etchants, and Secco and Wright are potentially decorating etchants.

Second, in an etchant bath as shown in Figure 37a, precipitate-free silicon wafers were etched by different etchants. The same hydrodynamic conditions were maintained for all etchants. The surface roughness as a function of the linear removal was recorded for each etchant (Figure 37b). Note that the parameters used for normalizing the surface roughness and the removal in this section (Section II) can be different from those used in the previous section (Section I). The polishing etchants reduce the surface roughness with increasing removal, whereas the potentially decorating etchants do not reduce the surface roughness. This experiment establishes MAE, $HF + HNO_3$, and $HF + HNO_3 + H_3PO_4$ as polishing etchants, and Secco and Wright as potentially decorating etchants. The data points inside the two ellipses in Figure 37b indicate very high roughness readings beyond the sensitivity of the roughness gauge used. Nevertheless, in this case, the roughness does not decrease with the removal, and, hence, the argument holds.

An Experimental Comparison between the Normal-Polishing and the Potentially Decorating Etchants. MAE, $HF + HNO_3$, and $HF + HNO_3 + H_3PO_4$ are classified as the polishing etchants and Secco and Wright are the potentially decorating etchants, according to the proposed models. A comparison among the decorating capacities of the aforementioned etchants can validate the model. The decorating performance of each etchant was experimentally verified by the standard procedure for the microdefect decoration. In all experiments discussed henceforth, different silicon wafers having similar native microdefect distribution were used. First, silicon wafers were saturated with copper at 900 °C and then cooled very quickly to room temperature. The fast cooling allows growth of the copper precipitate colonies on the microdefects. Some excess copper also escapes to the wafer surface and forms the tiny *surface copper precipitate colonies* during the cooldown. This wafer is then cleaned and polished to remove the surface copper precipitate colonies. Etching in any polishing etchant, such as MAE, accomplishes the surface polishing. Since the surface copper precipitate colonies exist only on the surface of a wafer after precipitation, even a normal-polishing etchant would erase the surface etch-pits formed by these colonies, given sufficient removal. Figure 38 shows the surface of a polish-etched wafer, using MAE. Since microdefect distributions in silicon wafers show azimuthal symmetry, only halves of any given wafer sample are used for these experiments. Figure 38 displays a digital image of the wafer visible to the naked eye, or the *macrophoto*, and an image of the wafer as seen under a Nomarski microscope, or the *microphoto*. A-defects are practically not decorated at all in the polishing step. A weak

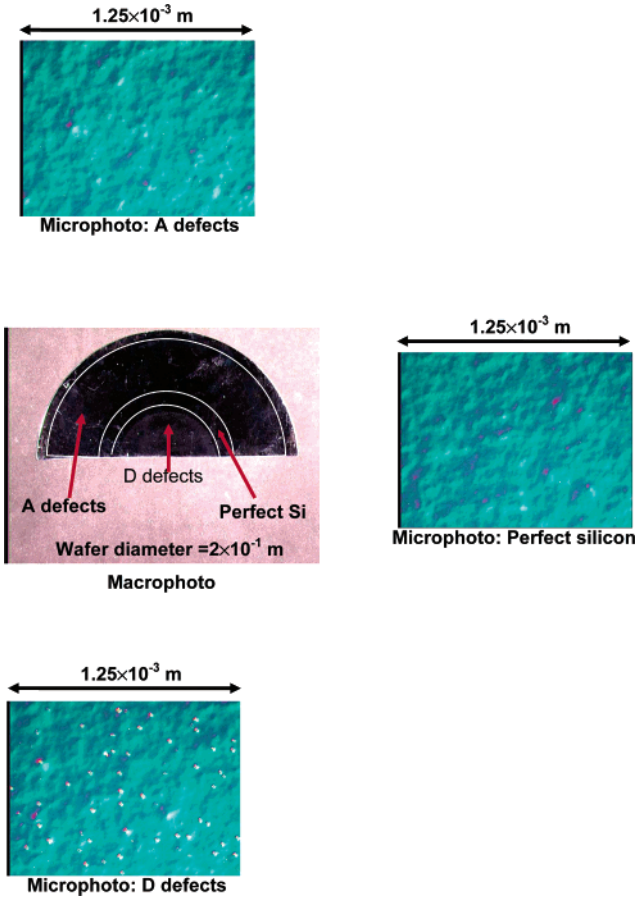

Figure 38. Microdefect-related etch-pits in the reference wafer after the copper precipitation and the surface polishing by MAE.[53] (Reproduced by permission of The Electrochemical Society, Inc.).

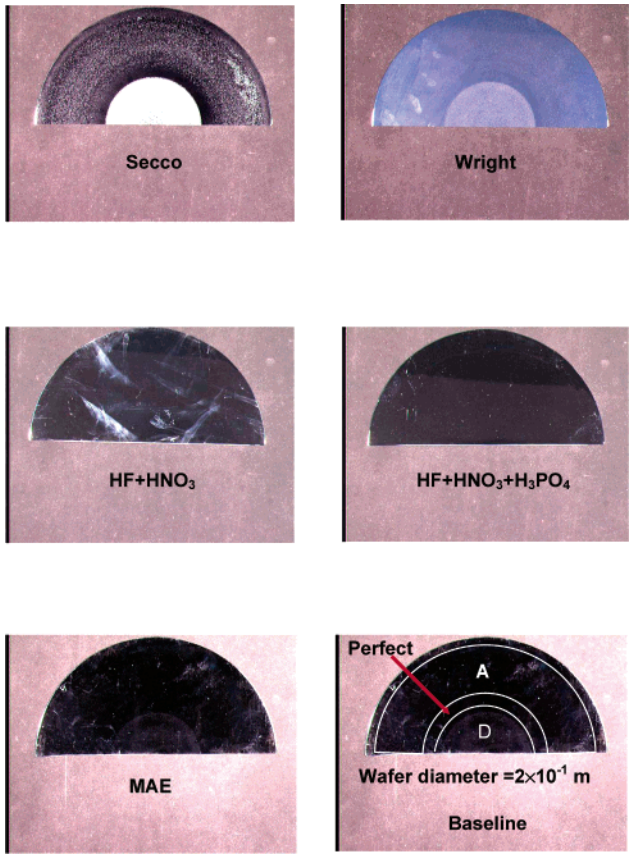

Figure 39. Macrophotos of the microdefect decoration by different etchants.[53] (Reproduced by permission of The Electrochemical Society, Inc.).

decoration of D-defects, however, indicates that MAE acts as a normal polishing etchant in the D-defect region. An etchant is defined as either decorating or polishing based on the microdefect patterns shown in Figure 38.

The wafers subjected to the copper precipitation and the surface polishing were then etched by the different etchants under consideration. Figure 39 shows a typical result of the microdefect decoration. It is evident that Secco and Wright are indeed the decorating etchants and MAE, HF + HNO_3, and HF + HNO_3 + H_3PO_4 are at least the normal-polishing etchants. This observation is further confirmed by the microphotos of the microdefect decoration (Figure 40).

On the basis of the kinetic and the hydrodynamic responses, the behavior of the different etchants under consideration is consistent with their classification as either potentially decorating or polishing. In addition, it can also be shown that a normal-polishing etchant erases or at least reduces the depth of the etch-pits created by a previous decoration by a decorating etchant. The following experiment of sequential processes tests this hypothesis:

copper precipitation → surface polishing →
decorating etching → polishing etching

Figures 41 and 42 show the results of this experiment. The macrophotos of a wafer after the Secco etching followed by the MAE etching are displayed in Figure 41. The macrophotos of a wafer after the Secco etching and the subsequent HF + HNO_3 + H_3PO_4 etching are also shown in Figure 41. Similar sequential experiments were conducted with Wright and HF + HNO_3 etchants and Wright and HF + HNO_3 + H_3PO_4 etchants. The reduction in the microdefect-related etch-pit depth by the polishing etchants is clearly illustrated by the microphotos shown in Figure 42. Hence, the hypothesis underlying the classification of the decorating and the polishing etchants based on the kinetic and the hydrodynamic conditions is verified.

Effect of Colonies of Copper Precipitates on Wafer Surfaces. A study of the effect of the copper precipitate colonies on wafer surfaces further verifies the proposed phenomenological model. As explained before, during the wafer cooldown after its saturation with copper at a higher temperature, copper out-diffusion to the wafer surface takes place, in addition to the Cu_3Si precipitate formation on the microdefects in the bulk silicon. The out-diffused copper forms tiny surface copper precipitate colonies. The formation of the surface copper precipitate colonies is afunction of the bulk microdefect density. If the bulk microdefect density is quite high, then a sufficient amount of copper precipitates on the bulk microdefects, resulting in a weak out-diffusion effect. Sufficient copper, however, out-diffuses to the wafer surface and forms dense (high-density) surface colonies, when the bulk microdefect density is lower.

The variation in the surface copper precipitate colony distribution as a function of the bulk microdefect density can be revealed using the principles of the proposed phenomenological model. For this purpose, two experi-

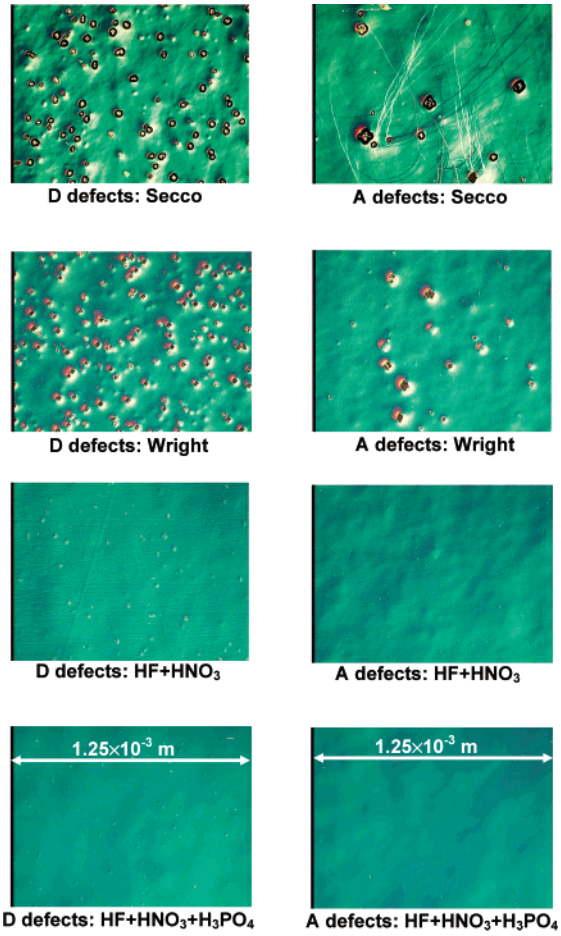

Figure 40. Microphotos of the microdefect decoration by different etchants.[53] (Reproduced by permission of The Electrochemical Society, Inc.).

ments involving different sequential processes were conducted:

(1) copper precipitation → polishing etching → decorating etching

(2) copper precipitation → decorating etching

Consider a local section of a wafer having low-density (not highly dense) A-defects. As explained before, the standard experiment described by the first set of processes above contains a surface-polishing step and, hence, allows elimination of the surface disturbances caused by the surface copper precipitate colonies (Figure 43a). Such a polishing step, however, is absent in the second experiment. The surface copper precipitate colonies generate etch-pits on the surface since the decorating efficiency in the presence of a copper precipitate is positive for a decorating etchant. Again, these surface pits move with the moving wafer surface during further removal, in the absence of a surface-polishing step. When a bulk microdefect is revealed in the form of a pit by the decorating etchant, it finds itself surrounded by many pits created by the surface copper precipitate colonies (Figure 43b).

The bulk microdefect density is quite high, however, in the D-defect region. Hence, the effect of the surface copper precipitate colonies is insignificant. Thus, a comparison between the results of the first and the second experiment reveals the presence of the high-density (dense) surface copper precipitate colonies only

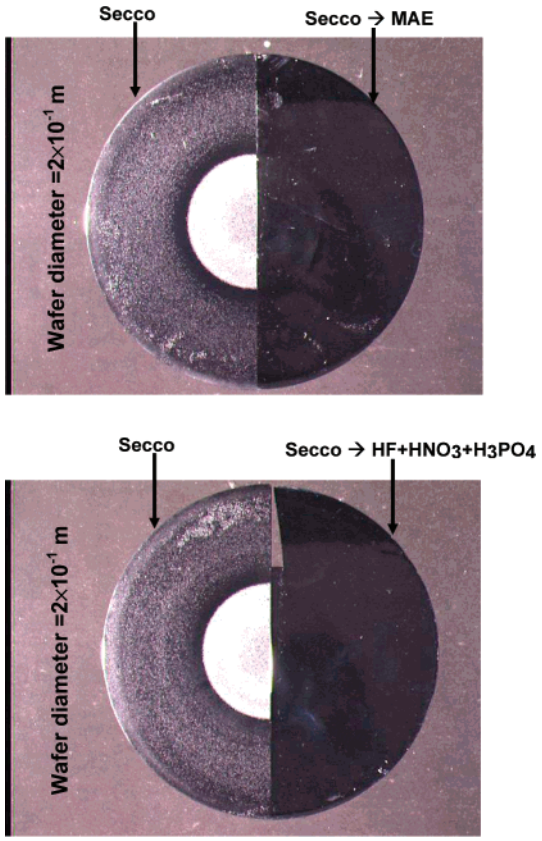

Figure 41. Erasure of the microdefect-related etch-pits by the polishing etchants: Macrophotos.[53] (Reproduced by permission of The Electrochemical Society, Inc.).

in the A-defect region. Figure 44 illustrates that the second experiment increases the surface density of the pits in the A-defect region, while the apparent change in the density of the etch-pits in the D-defect region is quite negligible. The kinetic and the hydrodynamic basis for identifying the polishing and the decorating etchants is verified by these experiments.

Conclusions: Sections I and II

Acid-based wet (liquid) etching is popularly applied in the manufacture of monocrystalline silicon substrate for device fabrication. Two key areas of its application are chemical surface polishing, to remove prior mechanical damage, and defect decoration. A unifying pseudo two-phase model built on the basis of a complex three-phase dynamics describes various aspects of the surface polishing and the defect decoration. At any given site on a silicon surface, various products of the etching reactions can form gaseous bubbles, which mask the site from further etching until they are dislodged into the liquid near the surface, through which the transport of reactants and products occurs. The masked site can form a peak if sufficient etching takes place on the surrounding unmasked sites. At a global level, the intense *bubble masking* leads to global surface irregularities. The entire three-phase dynamics can be represented by an equivalent etching system involving an effective reaction front on the wafer surface, to and from which the transport of reagents takes place through an effective mass-transport film in the liquid-phase. Both the molecular diffusion and the dispersion induced by the dislodged bubbles contribute to the transport through the effective mass-transport film.

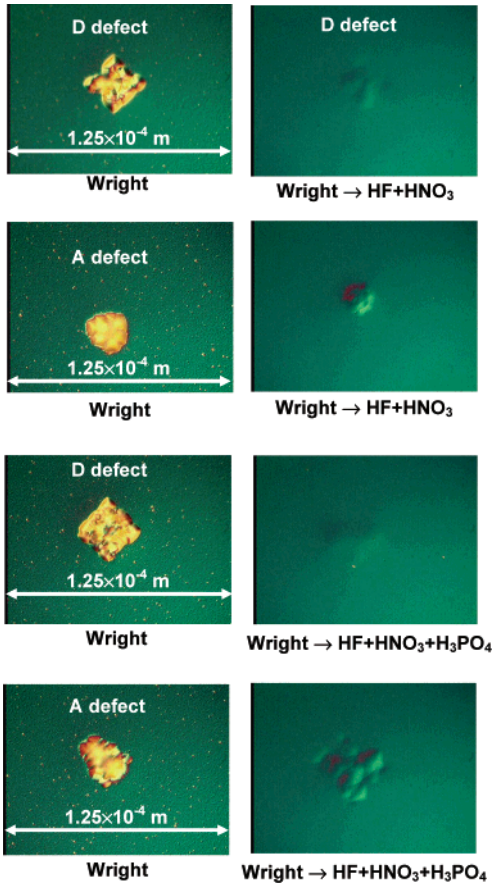

Figure 42. Erasure of the microdefect-related etch-pits by the polishing etchants: Microphotos.[53] (Reproduced by permission of The Electrochemical Society, Inc.).

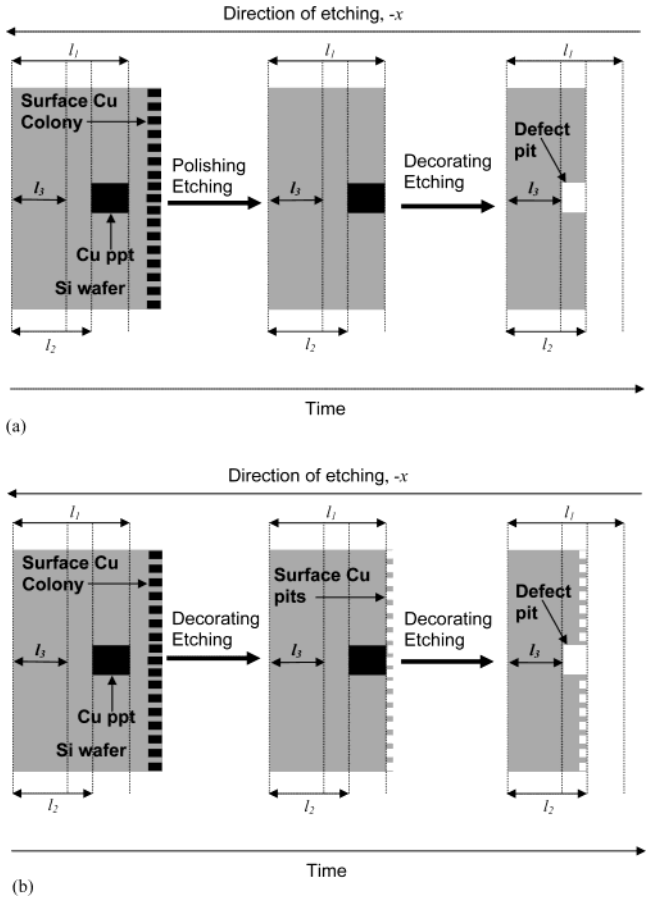

Figure 43. A schematic picture of (a) a standard microdefect decoration, (b) the surface roughening in the absence of the surface polishing.[53] (Reproduced by permission of The Electrochemical Society, Inc.).

The entire system can be modeled as a network of chemical resistances, across which various concentration-based driving forces drive the transport of all reagents. The reagents overcome the effective mass-transport resistance and the effective kinetic resistance, which act in series with each other, to complete the reaction. Parallel contributions from the effective molecular diffusion and the effective bubble-induced dispersion define the effective mass-transport resistance.

The conditions required for the intense bubble masking can be quantified by the ratio of the effective mass-transport resistance to the effective kinetic resistance. Mass-transport and kinetic influences on the etching process can be explained by the same ratio.

A rough silicon wafer is a field of peaks and valleys characterized by an average roughness. In a mass-transport-influenced system, the etching rates at peaks are higher than the etching rates at valleys as a result of the difference in the local effective mass-transport resistances. Thus, in the presence of the effective mass-transport resistance, chemical polishing takes place. Dependence of the polishing efficiency (the ratio of the actual polishing rate to the maximum possible polishing rate) on the ratio of the effective mass-transport resistance to the effective kinetic resistance can be explained using the proposed phenomenological model and the collected experimental data. The developed analytical expressions relate the polishing efficiency to the effective transport and the effective kinetic resistances; this relationship is physically meaningful when the scale of bubble masking is different from the scale of the roughness of interest. The system can be analyzed by studying three limiting cases, the first representing the variation of the effective mass-transport film thickness with liquid mixing intensity, the second representing the variation in the effective diffusivity of the key reactant by the addition of inert thickeners, and the third representing the variation in the effective kinetic resistance with the composition of the etchant. As the mixing intensity in the reactor decreases from infinity to zero, the polishing efficiency increases from zero to a maximum value and asymptotically approaches zero. As the effective diffusivity or the effective kinetic resistance of the key reagent decreases from infinity to zero, the polishing efficiency monotonically increases and reaches an asymptotic value. In practice, the polishing efficiency, which is a function of the ratio of effective mass-transport resistance to the effective kinetic resistance, can be controlled by varying either the HF or the thickener (phosphoric acid) concentration.

Generally, the etchants used for surface polishing are known as the polishing etchants and the etchants used for defect characterization or defect decoration are known as the decorating etchants. The interplay between the mass-transport effects and the surface kinetics in chemical etching of monocrystalline silicon can be quantified to define both the decorating and the polishing capacities of an etchant.

As a result of the difference between the etching rate of the microdefect site and that of the surrounding defect-free silicon, the decorating etching creates pits at the microdefect sites. Precipitation of copper as Cu_3Si particles around the microdefects, known as the copper

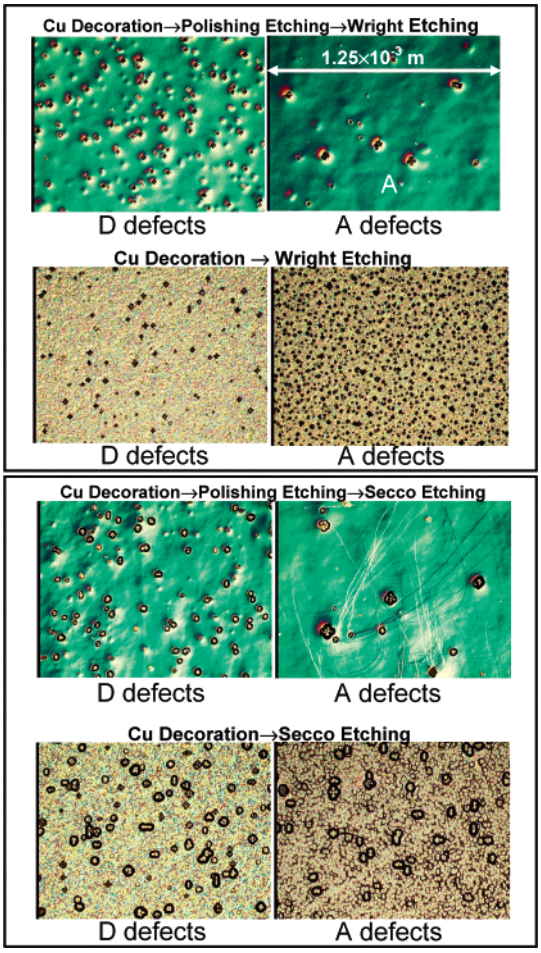

Figure 44. Effect of the surface copper precipitate colonies on the quality of the microdefect decoration.[53] (Reproduced by permission of The Electrochemical Society, Inc.).

precipitate colonies, improves the quality of the microdefect decoration. The decorating efficiency of an etchant at the microdefect site, defined as the ratio of the rate of increase in the microdefect related etch-pit depth to the maximum possible rate of increase in the pit depth, can be given as a function of the effective kinetic and the effective mass-transport resistances at the site and on the perfect (defect-free) silicon surface. The polishing efficiency of an etchant, defined as the ratio of the rate of decrease in the pit depth to the maximum possible rate of decrease, is also given as a function of these resistances. The effective mass-transport resistance and the effective kinetic resistance, in essence, influence the nature of an etchant.

Generally, the decorating efficiency decreases with an increase in the ratio of the effective mass-transport resistance to the effective kinetic resistance, although the variation of the decorating efficiency as a function of this ratio is complex. The decorating efficiency is zero when the sum of effective kinetic resistance and the effective mass-transport resistance at the microdefect site is equal to the sum of the effective kinetic resistance and the effective mass-transport resistance on the perfect silicon surface. A further increase in the mass-transport effects can result in the *crossover* from the decorating conditions to the polishing conditions.

In practice, the decorating efficiency can be controlled by varying the effective mass-transport film thickness, the effective liquid-phase diffusivity of reagents, or the effective kinetic resistance. Variations in the effective diffusivity and the effective kinetic resistance affect the decorating efficiency in the same way. The limiting asymptotic value of the decorating efficiency achieved with an infinitely thick effective transport film is different from that achieved when the effective diffusivity or the effective kinetic resistance is zero. A few aspects of generic behavior of the decorating efficiency and the crossover criteria, however, remain the same for all conditions.

In the presence of a weak polishing etchant, the microdefect decoration can exhibit *auto-inhibition* when the mass-transport effects are present but not dominant. A weak microdefect decoration takes place by the formation of shallow etch-pits under the auto-inhibiting conditions. As the etch-pit depth increases, however, the decorating efficiency decreases. The etch-pits are eventually erased after the complete dissolution of the copper precipitate colonies due to the polishing nature of the etchant in the absence of the copper precipitates. A site can make a transition from the microdefect-decorating conditions to the neutral conditions even before the complete dissolution of the copper precipitates, under the auto-inhibition. The maximum dynamic etch-pit depth at this transition under the auto-inhibiting conditions is given as a function of the microdefect kinetics, the surface kinetics, and the liquid-phase diffusivity.

The propagation of the etch-pits is as important as their formation for an efficient microdefect decoration. Therefore, the kinetic effects must be very dominant over the mass-transport effects to achieve an efficient microdefect decoration.

On the basis of their dependence on the reactor hydrodynamics, potentially decorating and polishing etchants can be identified. The etching rates of the polishing etchants show a strong dependence on the reactor hydrodynamics whereas the etching rates of the decorating etchants show a weak dependence on the hydrodynamics in the reactor. A decorating etchant preserves the surface irregularities whereas these irregularities are erased by a polishing etchant.

Acknowledgment

The author acknowledges Henry Erk, Jeffrey Libbert, Steven Keltner, and Luciano Muléstagno, who, along with the author, coauthored the papers published in *Journal of The Electrochemical Society*, from which much of the contents of this paper are drawn. The author thanks *The Electrochemical Society* for permitting the reproduction of the contents of the published papers. The author extends his appreciation to Judy Schmidt, Tom Doane, Shawn Patton, and Steve Mecker for performing the experiments. The author is grateful to MEMC in general and MEMC, Kuala Lumpur and Kalai Selvan in particular, for developing new etching processes based on this research.

Note Added after ASAP Posting

As a result of production errors, the paper was published ASAP on 4/18/03 with a minor typographical error and a missing label in Figure 33. A corrected version was posted on 4/25/03. Furthermore, a correction to eq 28 was posted on 5/20/03.

Literature Cited

(1) Shimura, F. *Semiconductor Silicon Crystal Technology*; Academic Press: San Diego, 1989; pp 184−186.

(2) Moldovan, N.; Ilie, M. From Atomic Parameters to Anisotropic Etching Diagrams. *Mater. Sci. Eng.* **1996**, *B37*, 146−149.

(3) Camon, H.; Moktadir, Z.; Djafari-Rouhani, M. New Trends in Atomic Scale Simulation of Wet Chemical Etching of Silicon with KOH. *Mater. Sci. Eng.* **1996**, *B37*, 142−145.

(4) Dyer, L. D.; Grant, G. J.; Tipton, C. M.; Stephens, A. E. A Comparison of Silicon Wafer Etching by KOH and Acid Solutions. *J. Electrochem. Soc.* **1989**, *136*, 3016−3018.

(5) Verhaverbeke, S.; Teerlinck, I.; Vinckier, C.; Stevens, G.; Cartuyvels, R.; Heyns, M. M. The Etching Mechanisms of SiO_2 in Hydrofluoric Acid. *J. Electrochem. Soc.* **1994**, *141*, 2852−2857.

(6) Kikuyama, H.; Waki, M.; Miyashita, M.; Yabune, T.; Miki, N. A Study of the Dissociation State and the SiO_2 Etching Reaction for HF Solutions of Extremely Low Concentration. *J. Electrochem. Soc.* **1994**, *141*, 366−373.

(7) Monk, D. J.; Soane, D. S. Determination of the Etching Kinetics for the Hydrofluoric Acid/ Silicon Dioxide System. *J. Electrochem. Soc.* **1993**, *140*, 8, 2339−2346.

(8) Schwartz, B.; Robbins, H. Chemical Etching of Silicon, III. A Temperature Study in the Acid System. *J. Electrochem. Soc.* **1961**, *108*, 4, 365−372.

(9) Bogenschütz, A. F.; Krusemark, W.; Locherer, K. H.; Mussinger, W. Activation Energies in the Chemical Etching of Semiconductors in HNO_3−HF−CH_3COOH. *J. Electrochem. Soc.* **1967**, *114*, 9, 970−973.

(10) Robbins, H.; Schwartz, B. Chemical Etching of Silicon, I. The System of HF HNO_3 and H_2O. *J. Electrochem. Soc.* **1958**, *106*, 505−508.

(11) Robbins, H.; Schwartz, B., Chemical Etching of Silicon, II. The System of HF HNO_3, H_2O and $HC_2H_3O_2$. *J. Electrochem. Soc.* **1960**, *107* (2), 108−111.

(12) Schwartz, B.; Robbins, H. Chemical Etching of Silicon, *J. Electrochem. Soc.* **1976**, *123*, 1903−1909.

(13) Klein, D. L.; D'Stefan, D. J. Controlled Etching of Silicon in the HF−HNO_3 System. *J. Electrochem. Soc.* **1961**, *108*, 1, 37−42.

(14) Erk, H.; Vandamme, R. Process and Apparatus for Etching Semiconductor Wafers. U.S. Patent, 5,340,437, 1994.

(15) Turner, D. R. Saturation Currents at n-Type Silicon and Germanium Electrodes in Chemical Etching Solutions. *J. Electrochem. Soc.* **1961**, *108*, 561−563.

(16) Nahm, K. S.; Seo, Y. H.; Lee, H. J. Formation Mechanism of Stains During Si etching Reaction in HF−Oxidizing Agen-H_2O Solutions. *J. Appl. Phys.* **1997**, *81*, 2418−2424.

(17) Schimmel, D. G.; Elkind, M. J. An Examination of the Chemical Staining of Silicon. *J. Electrochem. Soc.* **1978**, *125* (1), 152−155.

(18) Fathauer, R. W.; George, T.; Ksendzov, A.; Vasquez, R. P. Visible Luminescence from Silicon Wafers Subjected to Stain Etches. *Appl. Phys. Lett.* **1992**, *60*, 995−997.

(19) Gaffney, K.; Chiou, H. Achieving Super-Flat, Stain Free Wafers Through Acid Etching. *The 193rd Meeting of The Electrochemical Society, Inc., San Diego*, 1998; 98-1, Abstract 502.

(20) Bauer, Th.; Farbry, L.; Teuschler, T.; Schwab, G.; Stadler, M. Quality Aspects of Chemical Etching of Silicon Wafers. *The 193rd Meeting of The Electrochemical Society, Inc., San Diego*, 1998; 98-1, Abstract 321.

(21) Berishev, I. E.; De Anda, F.; Mishournyi, V. A.; Olvera, J.; Ilyinskaya, N. D.; Vasilyev, V. I• H_2O_2:HF:$C_4O_6H_6$ (Tartaric Acid):H_2O Etching System for Chemical Polishing of GaSb. *J. Electrochem. Soc.* **1995**, *142*, L189−L191.

(22) McAndrews, K.; Sukanek, P. C. Nonuniform Wet Etching of Silicon Dioxide. *J. Electrochem. Soc.* **1991**, *138*, 863−866.

(23) John, J. P.; McDonald, J. Spray Etching of Silicon in the HNO_3/HF/H_2O System. *J. Electrochem. Soc.* **1993**, *140*, 2622−2625.

(24) Osseo-Asare, K.; Wei, D.; Mishra, K. K. Dissolution Windows for Wet Chemical Processing of Silicon and Silicon Dioxide: Potential-pH Diagrams for the Si−F−H_2O System. *J. Electrochem. Soc.* **1996**, *143*, 749−751.

(25) Monk, D. J.; Soane, D. S.; Howe, R. T. Hydrofluoric Acid Etching of Silicon Dioxide Sacrificial Layers, I. Experimental Observations. *J. Electrochem. Soc.* **1994**, *141*, 264−269.

(26) Monk, D. J.; Soane, D. S.; Howe, R. T. Hydrofluoric Acid Etching of Silicon Dioxide Sacrificial Layers, II. Modeling. *J. Electrochem. Soc.* **1994**, *141* (1), 270−274.

(27) Monk, D. J.; Soane, D. S.; Howe, R. T. A Review of the Chemical Reaction Mechanism and Kinetics for Hydrofluoric Acid Etching of Silicon Dioxide for Surface Micromachining Applications. *Thin Solid Films* **1993**, *232*, 1−12.

(28) Kunii, Y.; Nakayama, S.; Maeda, M. Wet Etching of Doped and Nondoped Silicon Oxide Films Using Buffered Hydrogen Fluoride Solution. *J. Electrochem. Soc.* **1995**, *142*, 3510−3513.

(29) Aoyama, T.; Yamazaki; Ito, T. Nonuniformities in Chemical Oxides on Silicon Surfaces Formed during Wet Chemical Cleaning. *J. Electrochem. Soc.* **1996**, *143*, 2280−2285.

(30) Kulkarni, M. S.; Erk, H. F. Acid-Based Etching of Silicon Wafers: Mass-Transfer and Kinetic Effects. *J. Electrochem. Soc.* **2000**, *147*, 176−188.

(31) Levenspiel, O. *Chemical Reaction Engineering*; 2nd ed.; Wiley Eastern Limited: New Delhi, 1972; p 349.

(32) Perry, R. H.; Green, D. W. *Chemical Engineer's Handbook*, 6th ed.; McGraw-Hill: New York, 1984; p 4.1−4.91.

(33) Cussler, E. L. *Diffusion-Mass Transfer in Fluid Systems*; Cambridge University Press: Cambridge, 1984.

(34) Dash, W. C. Silicon Crystals Free of Dislocations. *J. Appl. Phys.* **1958**, *29*, 736.

(35) Dash, W. C. Growth of Silicon Crystals Free from Dislocations. *J. Appl. Phys.* **1959**, *30*, 459.

(36) Voronkov, V. V. The Mechanism of Swirl Defects Formation in Silicon. *J. Cryst. Growth* **1982**, *59*, 625.

(37) Abe, T.; Samizo, T.; Maruyama, S. Etch Pits Observed in Dislocation Free Silicon Crystals. *Jpn. J. Appl. Phys.* **1966**, *5*, 458.

(38) de Kock, A. J. R. The Elimination of Vacancy-Cluster Formation in Dislocation-Free Silicon Crystals. *J. Electrochem. Soc.* **1971**, *118*, 1851.

(39) Petroff, P. M.; de Kock, A. J. R. Characterization of Swirl Defects in Floating-Zone Silicon Crsytals. *J. Cryst. Growth* **1975**, *30*, 117.

(40) Föll, H.; Gösele, U.; Kolbesen, B. O. The Formation of Swirl Defects in Silicon by Agglomeration of Self-Interstitials. *J. Cryst. Growth* **1977**, *40*, 90.

(41) Roksnoer, P. J.; van den Boom, M. M. B. Microdefects in a Non-Striated Distribution in Floating-Zone Silicon Crystals. *J. Cryst. Growth* **1981**, *53*, 563.

(42) Sirtl, E.; Adler, A. Chromsäure-Flusssäure als Spezifisches System zur Ätzgrubenentwicklung auf Silizium. *Z. Mettalkd.* **1961**, *52*, 529.

(43) Secco d'Aragona, F. Dislocation Etch for (100) Planes in Silicon. *J. Electrochem. Soc.* **1972**, *119*, 948.

(44) Schimmel, D. G. A Comparison of Chemical Etches for Revealing ⟨100⟩ Silicon Crystal Defects. *J. Electrochem. Soc.* **1976**, *123*, 734−741.

(45) Jenkins, M. W. A New Preferential Etch for Defects in Silicon Crystals. *J. Electrochem. Soc.* **1977**, *124*, 757.

(46) Yang, K. H. An Etch for Delineation of Defects in Silicon. *J. Electrochem. Soc.* **1984**, *131*, 1140.

(47) Dash, W. C. Copper precipitation on Dislocations in Silicon. *J. Appl. Phys.* **1956**, *27*, 1193.

(48) de Kock, A. J. R., Microdefects in Dislocation-Free Silicon and Germanium Crystals. *Acta Electronica*. **1973**, *16*, 303.

(49) de Kock, A. J. R., Vacancy Clusters in Dislocation-Free Silicon. *Appl. Phys. Lett.* **1970**, *16*, 100.

(50) Graff, K. *Metal Impurities in Silicon-Device Fabrication*; Springer-Verlag:: Berlin, 2000; pp 98−105.

(51) Murarka, S. P.; Verner, I. V.; Gutmann, R. J. *Copper-Fundamental Mechanisms for Microelectronic Applications*; John Wiley and Sons: New York, 2000.

(52) Muléstagno, L.; Falster, R. Private communication, 1999.

(53) Kulkarni, M. S.; Libbert, J.; Keltner S.; Muléstagno, L. A Theoretical and Experimental Analysis of Macro-decoration of Defects in Monocrystalline Silicon. *J. Electrochem. Soc.* **2002**, *149* (2), G153−165.

Received for review September 12, 2002
Revised manuscript received January 21, 2003
Accepted January 21, 2003

IE020716Y